FUNDAMENTAL INVESTIGATION OF LIQUID-METAL LUBRICATED JOURNAL BEARINGS

Quarterly Technical Report No. 3
Contract No. AT(11-1)-1228
Project Agreement No. 8
Modification No. 7

R.A. Burton
H.J. Carper
Y.C. Hsu
P.A. Hunter

to

U.S. Atomic Energy Commission
Washington 25, D.C.

January 14, 1965

Report No. RS-440

SOUTHWEST RESEARCH INSTITUTE
SAN ANTONIO HOUSTON

DISCLAIMER

SOUTHWEST RESEARCH INSTITUTE
8500 Culebra Road, San Antonio, Texas 78206

Department Of Aerospace Propulsion Research

FUNDAMENTAL INVESTIGATION OF LIQUID-METAL LUBRICATED JOURNAL BEARINGS

Quarterly Technical Report No. 3
Contract No. AT(11-1)-1228
Project Agreement No. 8
Modification No. 7

R.A. Burton
H.J. Carper
Y.C. Hsu
P.A. Hunter

to

U.S. Atomic Energy Commission
Washington 25, D.C.

January 14, 1965

APPROVED:

for Ralph Burton

P.M. Ku, Director
Department of Aerospace
Propulsion Research

Report No. RS-440

TABLE OF CONTENTS

LIST OF SYMBOLS

a	Attitude parameter of bearing pad
a_1	Slope of anemometer calibration curve
b	Half-thickness of film
$\bar{C}$	Dimensionless location of center of pressure under bearing pad.
C_f	Friction coefficient
h	Film thickness
h_o	Bearing radial clearance
H	h/h_o
I	Anemometer current reading
I_o	Anemometer current reading for zero flow velocity
ℓ	Mixing length
m	Velocity profile parameter
N	Pressure at entry to bearing pad
n	Friction coefficient variation parameter
p	Pressure
P	Dimensionless pressure $(p/\rho u_b^2)$
r	Journal radius
R	Reynolds number ub/ν based on centerline velocity
u	Velocity in direction of turning
Δu	Incrementation of velocity relative to Couette flow

INTRODUCTION

This progress report summarizes the third quarter of a one-year program of basic research on liquid metal lubricated bearings, with emphasis on turbulent-film lubrication. In the initial progress report, the general problem was outlined along with the objectives of the program, and preliminary apparatus and experimental plans were described. In the second progress report, preliminary data were presented, and preliminary approaches to the analysis of turbulent film lubricated bearings were outlined. In this progress report, emphasis is on improved data and improved analyses on the major aspects of the problem. In many cases, these improvements represent the completion of sub-tasks of the program.

Highlights of Progress Report No. 3

Improved Friction Coefficient Data. In Progress Report No. 2, techniques were outlined whereby friction coefficient could be computed through use of the wall law along with velocity profile measurements. It was indicated that the wall law would be expected to apply with increasing accuracy as the position of the measurement was moved in toward the wall. It was also pointed out that the errors in the measurement would be expected to increase as the position of the velocity measuring probe was moved in toward the wall. Thus a compromise was required. In this report, an improved means of making this compromise has been arrived at: the wall law is applied blindly to all measurements across the channel, and a

friction coefficient is computed for each individual measurement. These friction coefficients are plotted and graphically extrapolated back to the wall. The resulting "wall" friction coefficients have been plotted against Reynolds numbers, and they appear to bear a logical relationship to prior work of Taylor, Smith and Fuller, Robertson, Couette, and others.

Improved Profile Analysis. This effort consists of two parts, one of which has been to find a suitable expression for the turbulent wall-law velocity profile, and the other is to compare the actual measured velocity profiles with the wall-law profile. In Progress Report No. 2, a simple expression was suggested as a close fit of wall-law data, and this expression has been explored more fully, showing it to be a much stronger representation than was initially expected. For example, the mixing length relationship carried implicitly in this expression is shown to be consistent with Emmons' observations on eddy dimensions. Comparison of the measured velocity profiles with the wall-law profile have shown, on the basis of the above local friction coefficient estimates, that there is an additional momentum transfer term in the flow in our large-scale turbulent film apparatus. This additional momentum transfer term is attributed to vortex flow which co-exists with the fully-turbulent flow.

Improved Pressure Measurements on the Full-Bearing Configuration in the Large-Scale Turbulence Apparatus. A new method for measurement of the extremely low pressures (as encountered in the full-scale bearing) was presented in Progress Report No. 2. This pressure

measurement technique has been further developed and exploited, and complete pressure profiles for the full bearing have been produced at three Reynolds numbers. Difficulties were encountered due to the relatively large magnitude of the velocity pressure, as compared with the static pressure which was being measured. Small disturbances in the flow, which changed the velocity, could alter the local static pressure significantly. Elaborate experimental care has removed this source of error, and it is believed that representative pressure profiles have been obtained.

Data on Skewed Flows. One of the most sought for items in this program has been data on strongly skewed flows. The relationship of velocity and shear stress has not previously been established experimentally for such flows, and any theoretical calculation is based primarily upon some assertion as to how the friction law should vary for such flows.

During this report period an obstruction was placed in the bearing film in the large-scale turbulence apparatus, and a wide variety of skewed profiles resulted. Both pressure measurements and profile measurements are reported here, and are expected to be subject to analysis in the forthcoming period.

Improved Derivations for Turbulent-Film Bearing Analysis. Derivations presented schematically in Progress Report No. 2 are reviewed and improved or corrected in many details.

Estimation of Inertial Effects in Pad-type Bearings. The analytical techniques outlined above have been extended to pads without end leakage, and with inertial effects. These include both the initial impact pressure at pad entry, and the continuous inertial effect throughout the film. The result of these computations is that the impact pressure is overwhelmingly significant in determing both center-of-pressure location, and load support for a variety of pad length-to-clearance ratios, and angles of incidence. It is expected that measurements of the actual impact pressure at pad entry will be available to support or correct these analyses in the forthcoming quarter.

FRICTION-COEFFICIENT VARIATION IN COUETTE FLOW

Friction Coefficient Variation

As pointed out in Progress Report No. 2, a program has been developed to determine the C_f and/or τ necessary to force experimental data to satisfy the universal velocity profile equation

$$Y^+ = U^+ + (U^+/8.74)^7 \tag{1}$$

or

$$y\sqrt{\tau/\rho}\Big/\nu = u\sqrt{\rho/\tau} + (u\sqrt{\rho/\tau}\Big/8.74)^7 \tag{2}$$

Here ν, ρ, y, and u are known, and τ may be solved for. If the actual profile is of the same form as the universal velocity profile, and if the flow is simple Couette flow, the value of C_f computed for any pair of (u, y) coordinates will correspond to that for any other pair. If the values of computed τ vary out from the wall, this indicates that the velocity profile does not follow the universal velocity profile.

Figure 1 shows a number of profiles of computed C_f (where $C_f \equiv 2\tau/\rho u_b^2$), showing the computed value to remain nearly constant, but still dropping off toward midstream. This tells us that the universal-velocity-profile shear-stress relationship underestimates the actual midstream shear stress; thus it indicates that an additional mode of momentum transfer must be at work, over and above the turbulent mode. This is undoubtedly Taylor vortex flow, still at work even when the flow is fully turbulent.

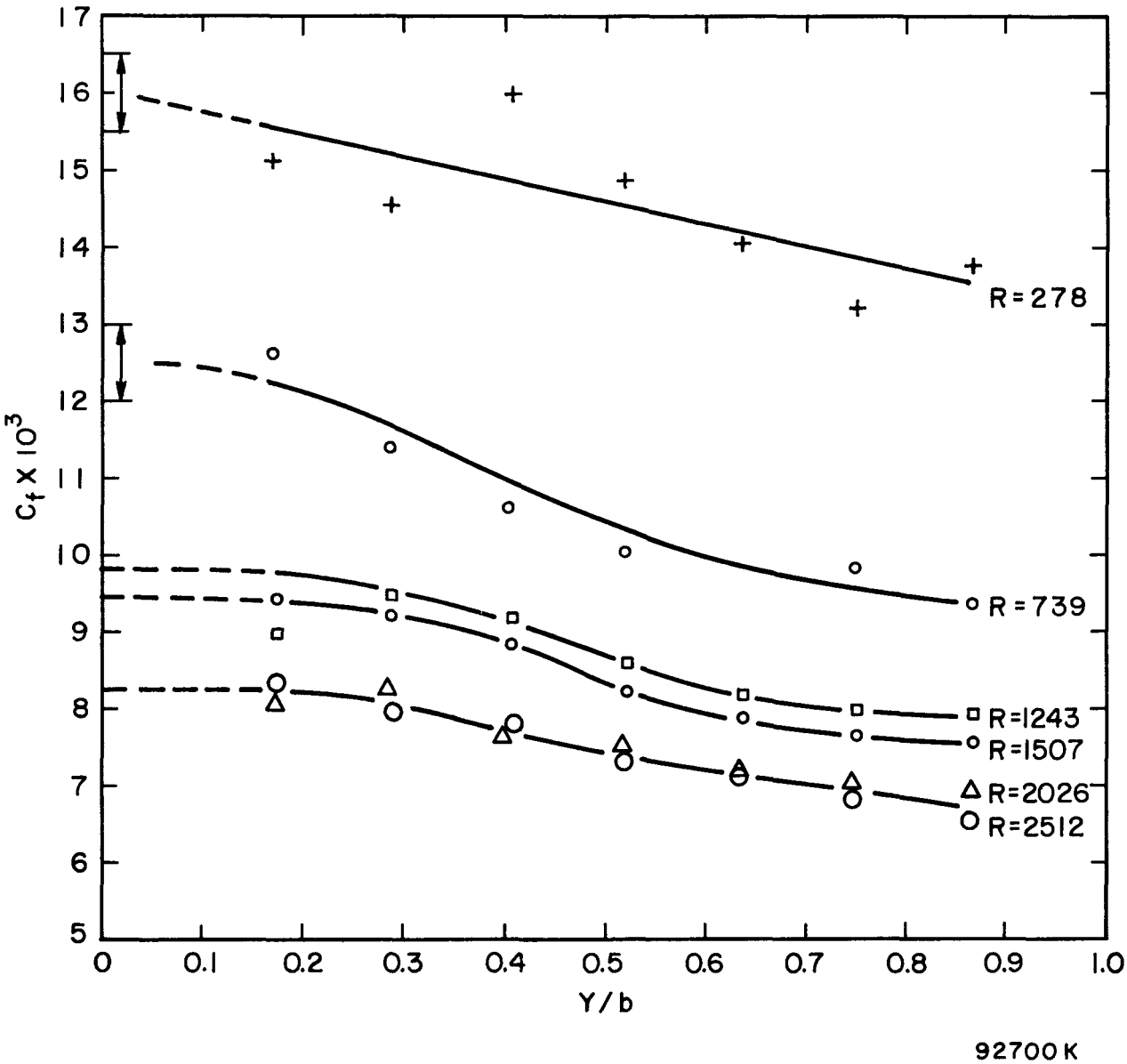

FIGURE 1. COMPUTED FRICTION COEFFICIENT BASED ON ASSUMED WALL-LAW PROFILE AS A FUNCTION OF DIMENSIONLESS POSITION IN CHANNEL AND REYNOLDS NUMBER

Extrapolations of the C_f plots back to the wall provided values which must be independent of this extra momentum transfer. The results of such extrapolations are plotted in Figure 2, and it is seen that the C_f magnitudes are above those for plane-Couette flow as well as the thin-film values of Smith and Fuller. The data tend toward the earlier data of Taylor for even thicker films, though the transition is at high Reynolds number. Critical Taylor number for transition is at $R \doteq 100$, and appears to correspond well to the observed transition.

In the forthcoming period, checks will be made to determine if similar effects take place under finite pads; and, if this is verified, a series of C_f profiles for different clearance/radius ratios will be reported.

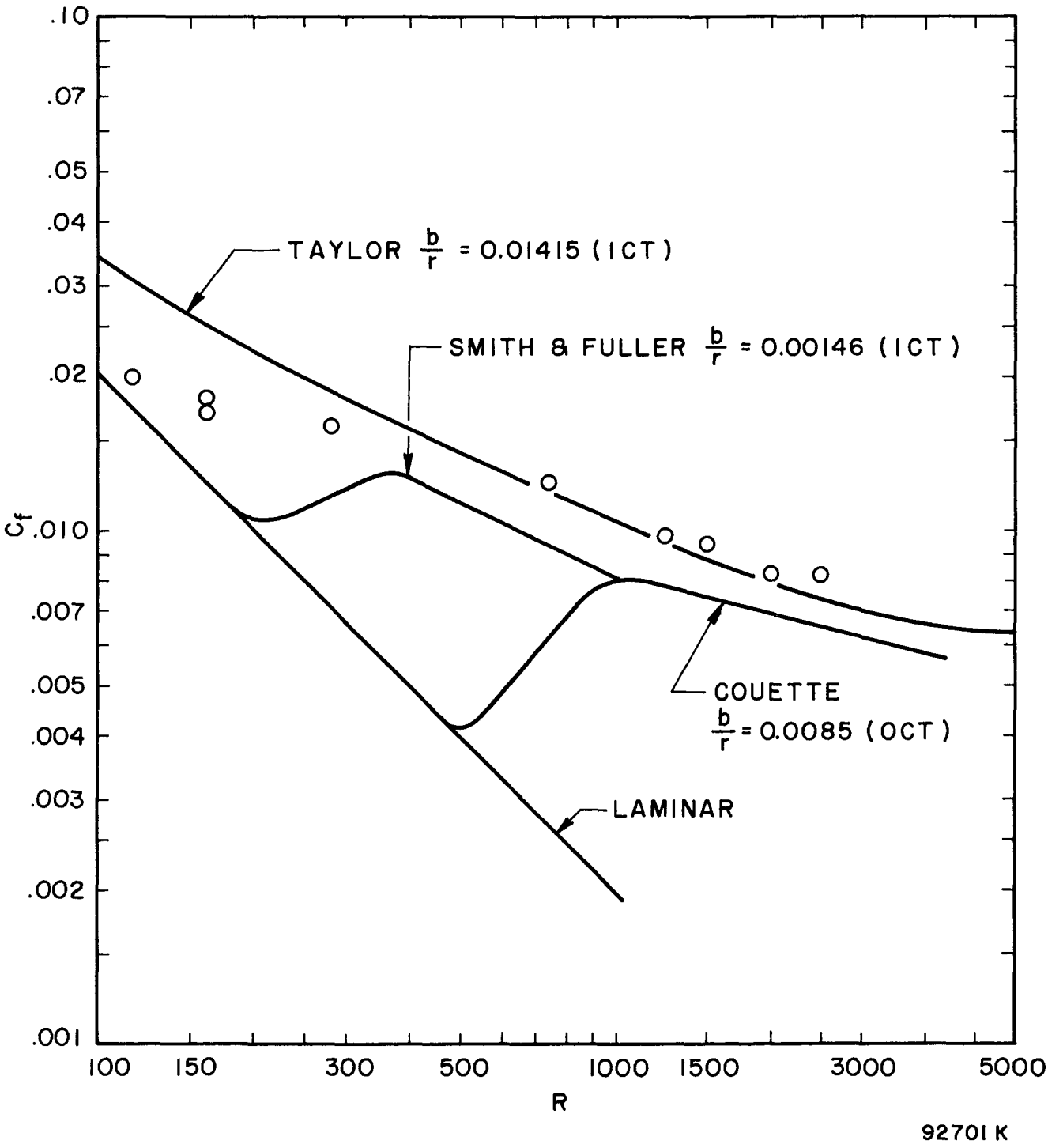

FIGURE 2. FRICTION COEFFICIENT AS A FUNCTION OF REYNOLDS NUMBER IN LARGE-SCALE TURBULENCE APPARATUS (b/r - 0.00793)

COMMENTS ON THE RECOMMENDED UNIVERSAL VELOCITY-PROFILE EQUATION

Numerous authors have attempted to fill the need for a continuous universal velocity profile expression, reaching all the way from the wall out into the turbulent flow. These include Miles[1], Van Driest[2], Szablewski[3], Reichardt[4], and Ng[5]. Aside from the fact that none of these precisely represents the others, all are relatively difficult functionally, and make hand calculation virtually impossible, when one tries to use them to compute shear stress from velocity data. To provide a simpler expression for such work, we have proposed the expression

$$Y^+ = U^+ + (U^+/8.74)^7 \qquad (1)$$

Here $U^+ = u\sqrt{\rho/\tau}$ and $Y^+ = (y/\mu\sqrt{\tau\rho})$, where u is velocity parallel to the wall, y is the coordinate normal to the wall, ρ is fluid density, τ is wall shear stress, and μ is viscosity. Somewhat unexpectedly, this relationship was found to fit available experimental data well. As shown in Progress Report No. 2, it follows the data of Nikuradse[6] up to a value of $Y^+ = 500$ and possibly as high as $Y^+ = 1000$. In the transition region near $Y^+ = 10$, it was shown also to agree closely with the data of Reichardt and Laufer. There is exceptionally good agreement between the selected function and Laufer's data, and it would be very satisfying if we could convince ourselves that these recent measurements are the most accurate.

Defining $C_f \equiv 2\tau/\rho u^2$, and $R \equiv uy/\nu$

Eq. (1) leads to the following friction law

$$R = \frac{2}{C_f} + \frac{(2/C_f)^4}{(8.74)^7} \tag{2}$$

A defining equation for eddy viscosity, η, may be written as follows

$$(\mu + \rho\eta)\frac{\partial u}{\partial y} = \tau \tag{3}$$

The shear stress τ may be assumed constant, since this is one of the essential conditions of the universal velocity profile. Combining Eq. (1) and Eq. (3), and drawing upon the appropriate definitions

$$\frac{\rho\eta}{\mu} = 0.801\,(U^+/8.74)^6 \tag{4}$$

Mixing length, ℓ, may be defined by

$$\eta = \ell^2 \left|\frac{\partial u}{\partial y}\right| \tag{5}$$

Combining this with the above relationship for eddy viscosity [Eq. (4)], and defining $\tau\ell^2/\rho\nu^2 \equiv L^2$

$$(L^+)^2 = 0.801\,(U^+/8.74)^6\,[1 + 0.801\,(U^+/8.74)^6] \tag{6}$$

It is not convenient to solve this explicitly for L^+ in terms of Y^+, but for the special cases of very large and very small Y^+ this becomes respectively:

For large Y^+

$$L^+ = 0.801\,(U^+/8.74)^6 = 0.801\,(Y^+)^{6/7} \tag{7}$$

For very small Y^+

$$L^+ = \sqrt{0.801}\,(\nu^+/8.74)^3 = \sqrt{0.801}\,(Y^+/8.74)^3 \tag{8}$$

Note that for the very small Y^+ this follows a cubic relation, for which Emmons[7] has given some substantiation in terms of reported measurements of eddy dimension. At the higher values of Y^+ the relationship is very nearly linear, as is ordinarily assumed in mixing length theory. The relationship between L^+ and Y^+ is best illustrated in Figure 3, where the predictions of Eq. (6) combined with Eq. (1), are shown merging into the cubic relationship at the small Y^+, and approaching (very nearly paralleling) the ordinarily assumed mixing length relationship of $L^+ = 0.4Y^+$. On the basis of these observations, we suggest that the simple profile represented by Eq. (1) not only provides a good direct fit of empirical velocity profile data, but also appears to make sense when viewed in terms of the mixing length relationship which it carries with it implicitly.

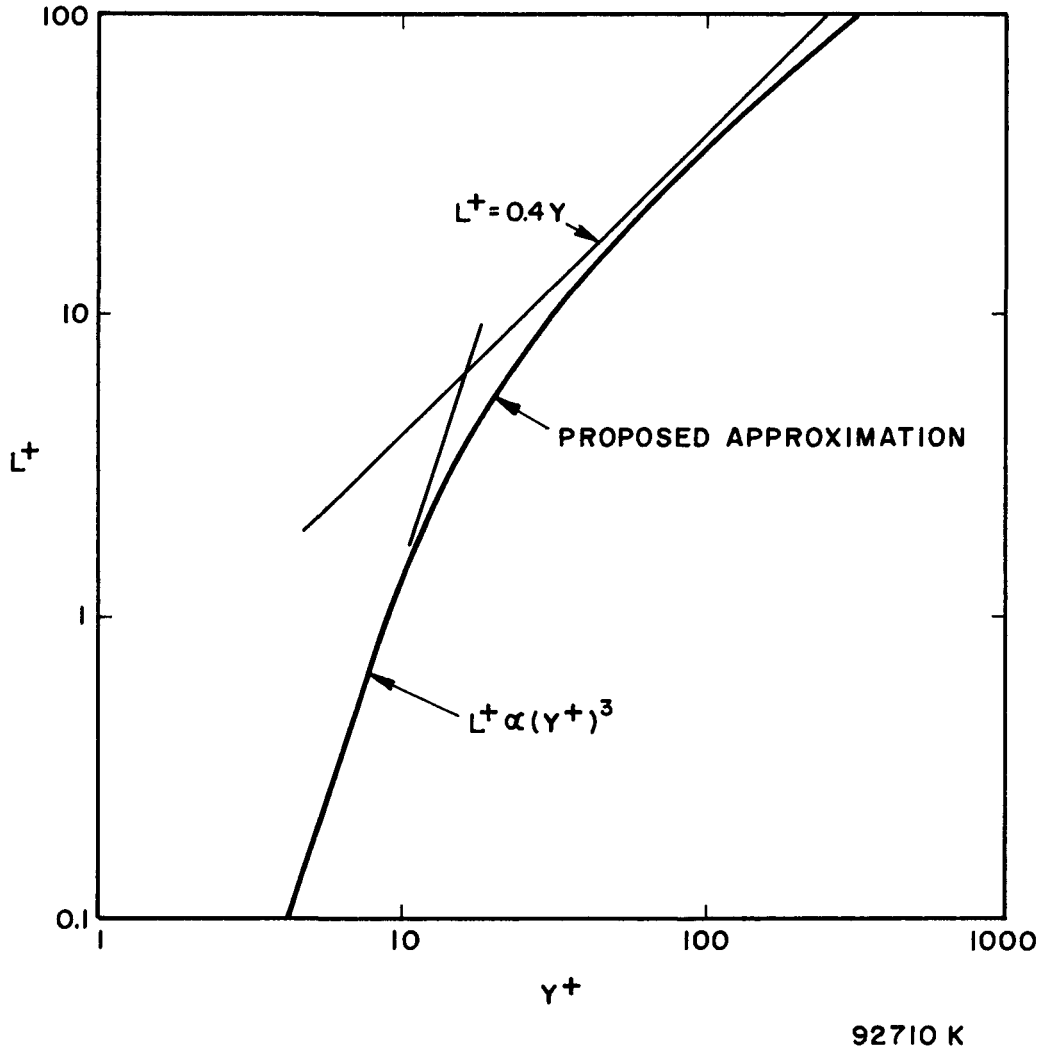

FIGURE 3. PLOT OF DIMENSIONLESS MIXING LENGTH

EMPIRICAL REPRESENTATION OF VELOCITY PROFILES

At the outset of the experimental program it was decided that the measured velocity profiles would be characterized by a best-fit power-law expression. To this end a least-squares technique was worked out for computer-analysis of the data.

In the past quarter, this has been re-assessed, and, to a large extent, abandoned. A graphical curve-fit appears to offer a preferable approach. The principal difficulties have been encountered at low values of R. In fact, the technique is quite satisfactory at large R or fully turbulent flow.

Figures 4 and 5 illustrate the agreement of the curve of the type $u/u_b = (y/b)^n$, for the n computed by the least-squares program, and for a relatively high Reynolds number. In this case, the fit is satisfactory on both linear and logarithmic plots.

Figures 6 and 7 show the results of three different techniques of arriving at the best exponent for the short profile at a low Reynolds number. It is seen that the least-squares result gives excessive weight to the single deviant point near the wall. An "eyeball" fit on the logarithmic plot (with emphasis on the points near midstream) also does not provide a satisfactory fit on the linear plot. As a third approach, one point at the knee of the curve was established accurately by repeated runs, and the power-law curve was computed to pass through this point. It appears that this last device is an effective approach to the problem of arriving at a single-parameter power-law for comparative purposes.

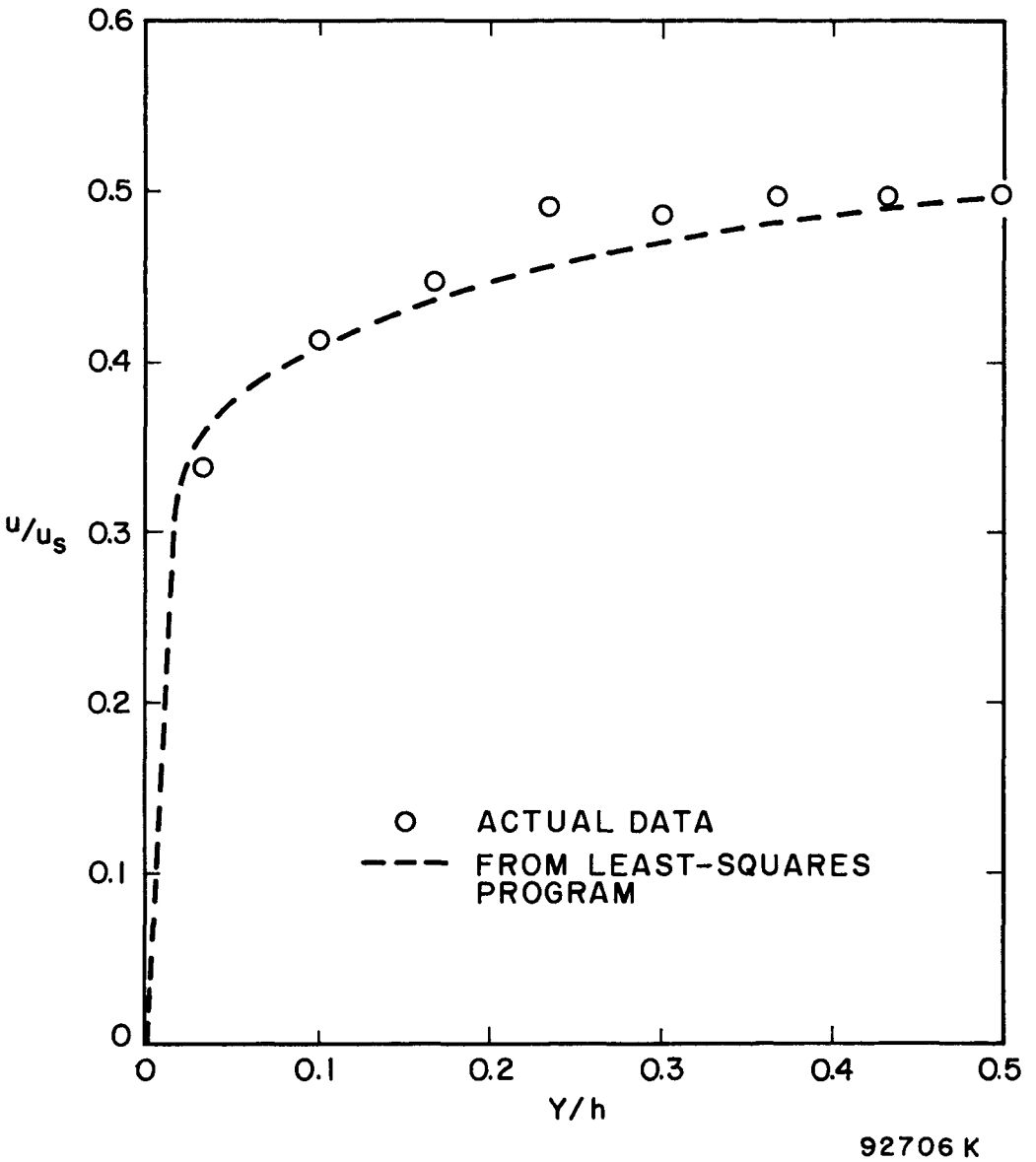

FIGURE 4. COMPARISON BETWEEN EXPERIMENTAL DATA AND LEAST-SQUARES CURVE FOR R = 2500

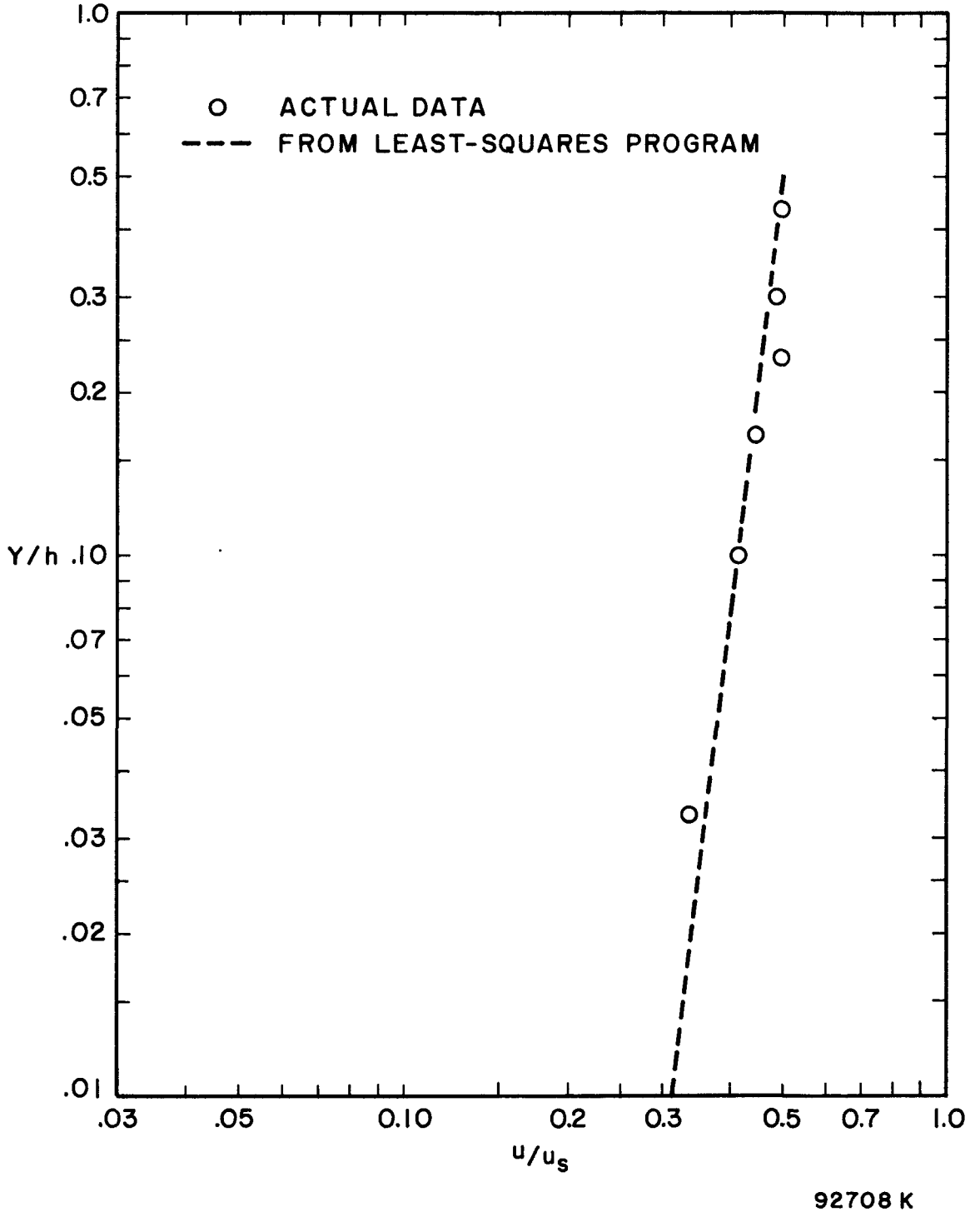

FIGURE 5. COMPARISON BETWEEN EXPERIMENTAL DATA AND LEAST-SQUARES CURVE FOR R=2500 - LOGARITHMIC PLOT

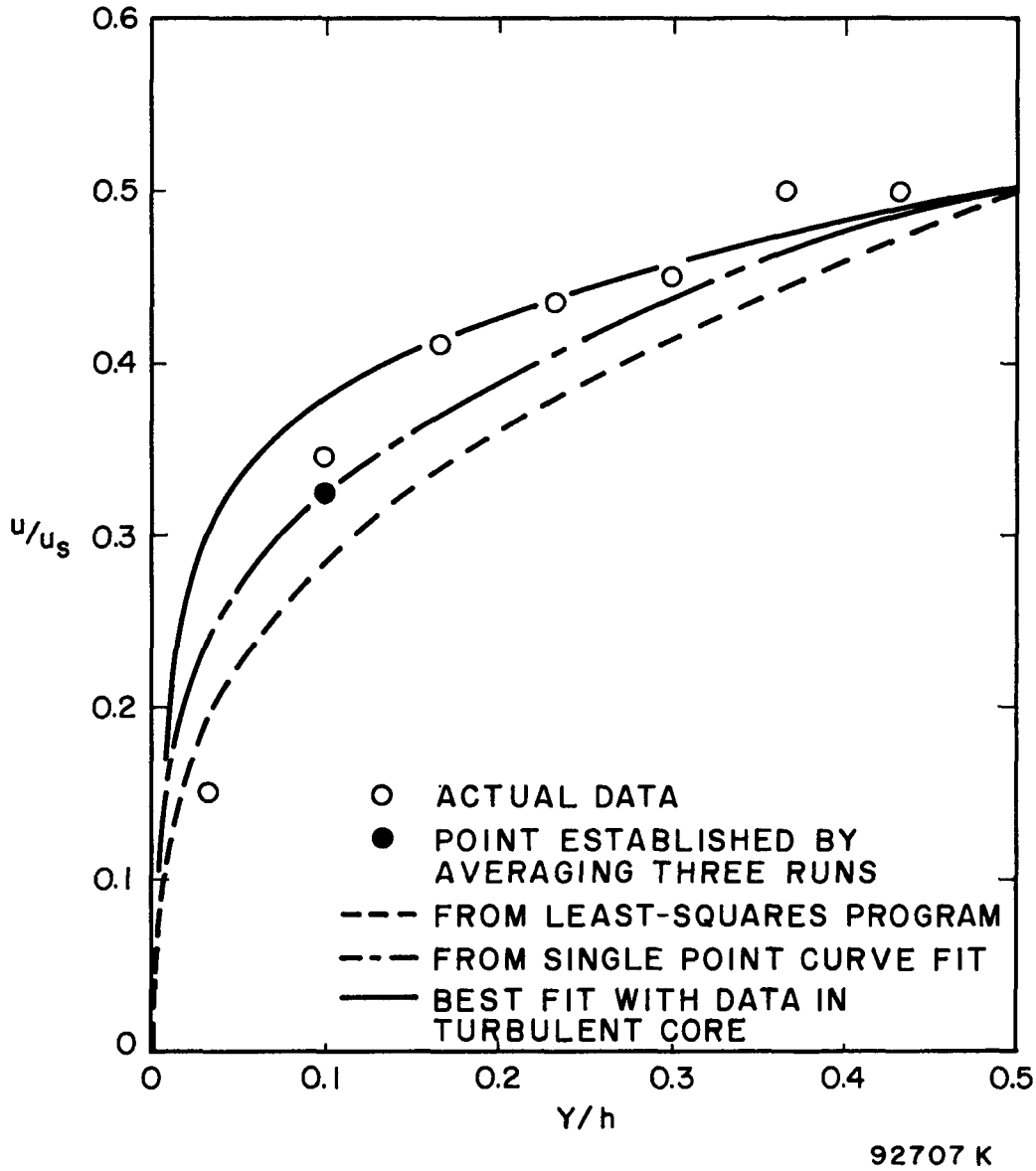

FIGURE 6. COMPARISON BETWEEN EXPERIMENTAL DATA AND THREE APPROACHES TO CURVE FITTING AT R = 740

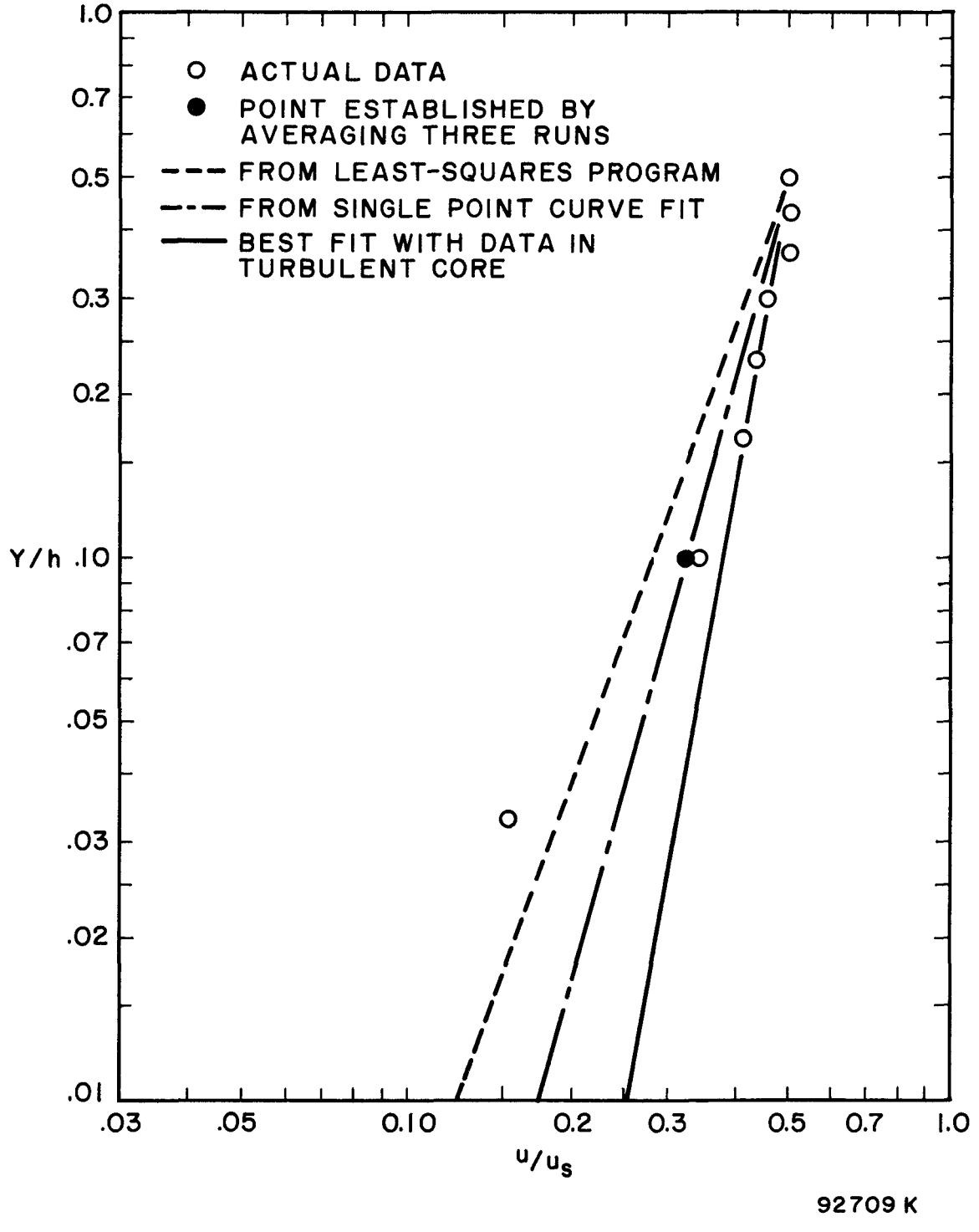

FIGURE 7. COMPARISON BETWEEN EXPERIMENTAL DATA AND THREE APPROACHES TO CURVE FITTING AT R=740 - LOGARITHMIC PLOT

Yet another approach to data analysis is shown in Figure 8, where actual profiles are compared with the universal velocity profile curve. To this end friction coefficient was computed by the extrapolation technique (See Figure 1), and this was used in computing Y^+ and U^+. In this case

$$U^+ = (u/u_b)\sqrt{2/C_f} \tag{9}$$

$$Y^+ = yR/U^+b \tag{10}$$

When plotted as shown, the midstream values (y = b) are below the universal velocity profile. This again emphasizes that some factor other than simple turbulence contributes to the resistance to flow.

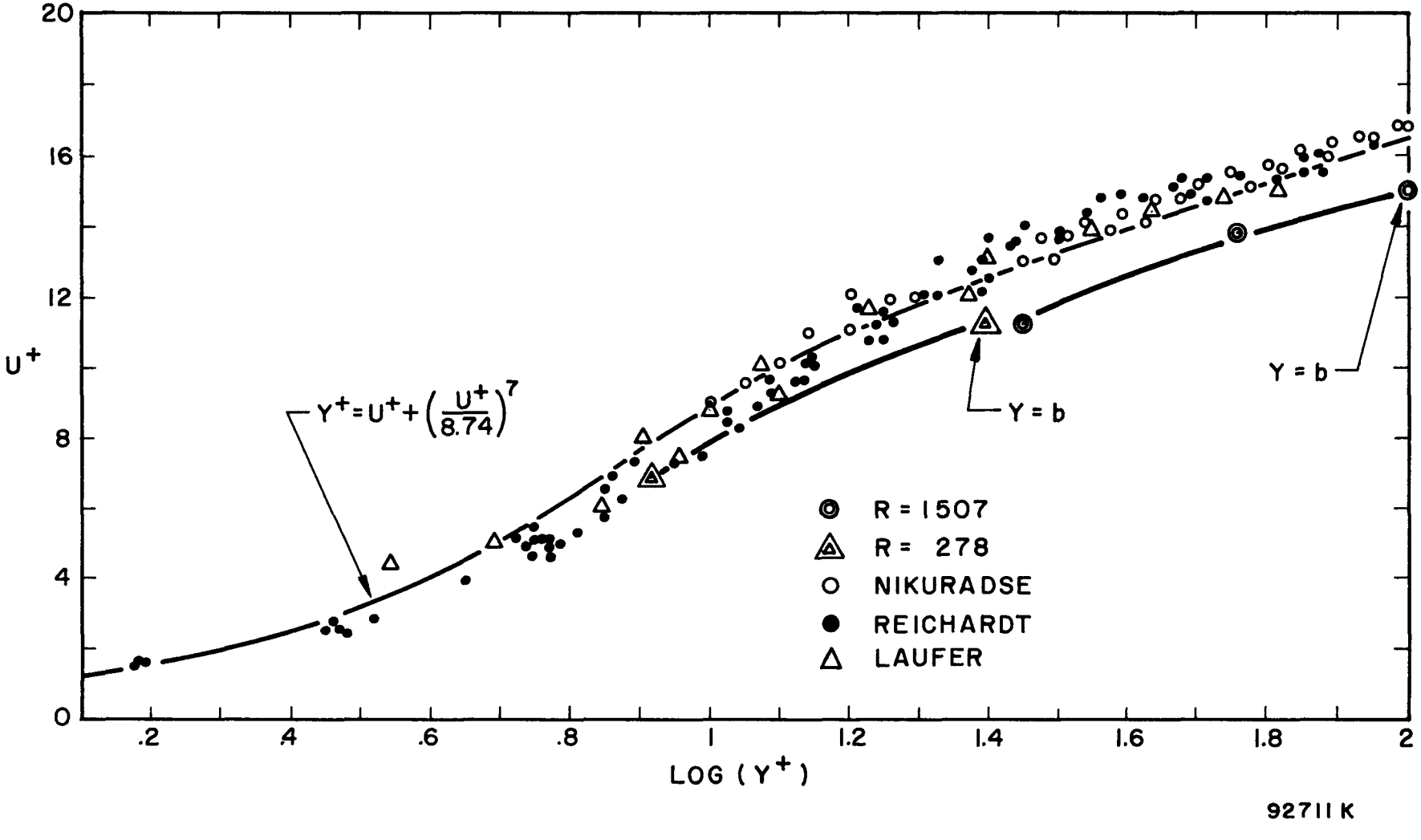

FIGURE 8. COMPARISON BETWEEN MEASURED PROFILES AND THE UNIVERSAL VELOCITY PROFILE

COMMENTS ON A NEWLY INTRODUCED METHOD FOR DEALING WITH TURBULENT SHEAR FLOWS IN BEARINGS

Recently Pan and Ng[5] have reported the application of a novel relationship for generation of velocity profiles in pressure flows, this having been suggested by Elrod. It is apparent that this relationship does, in general, fit the principal requirements of the problem. However careful analysis is required to assess it relative to other approaches such as the mixing-length approach. In essence, it is assumed that the eddy viscosity, η, bears a fixed relationship to Y^+, where $Y^+ = y\sqrt{\tau/\rho}/\nu$ rather than the more conventional $Y^+ = y\sqrt{\tau_o/\rho}/\nu$. In order to get eddy viscosity in any circumstance, the distribution that satisfies the wall law may be used to establish the functional relationship between Y^+ and $\rho\eta/\mu$. The exact function depends upon how well the wall law expression for $\rho\eta/\mu$ may be written. If we may apply the relationship from the previous section with confidence, we may write

$$\rho\eta \doteq (0.8)\,\mu(U^+/8.74)^6 \tag{11}$$

Or, in the fully-turbulent part of the flow (i.e., outside the sublayer)

$$\rho\eta \doteq 0.8\,\mu(Y^+)^{6/7} \tag{12}$$

With this simple relationship, it is possible to explore more fully the implication of this suggestion in flow where τ is a function of y. For example, it is particularly informative to determine the mixing-length relationship implied.

For flow when the viscous resistance is negligible

$$\tau = \rho \ell^2 (\partial u / \partial y)^2$$

In terms of eddy viscosity this is

$$\rho \eta \frac{\partial u}{\partial y} = \tau$$

Combining these

$$\ell = \sqrt{\rho/\tau}\ \eta \tag{13}$$

Using Eq. (12) for η

$$\ell = \sqrt{\rho/\tau}\ (0.8)\ \mu\, [(y/\nu)\sqrt{\tau/\rho}]^{6/7} \tag{14}$$

For Couette flow where $\tau = \tau_o$, this would be

$$\ell_c = \sqrt{\rho/\tau_o}\ (0.8)\ \mu [(y/\nu)\sqrt{\tau_o/\rho}]^{6/7} \tag{15}$$

Comparing a flow with varying τ to the Couette flow, for corresponding values of y

$$\frac{\ell}{\ell_c} = \left(\frac{\tau_o}{\tau}\right)^{1/14} \tag{16}$$

This would call for $\ell \to \infty$ when $\tau \to 0$ (as at midstream of pure pressure flow). On the other hand this is not serious since $\eta \to 0$ when $\tau \to 0$, thus giving a realistic profile. Over most of the range the $(\tau/\tau_o)^{1/14}$ is such a weak function that $\ell \to \ell_c$ and the assumption is equivalent to a fixed mixing length distribution, corresponding to that for the universal velocity profile (or for Couette flow). This is especially true for small-perturbation pressure flow imposed upon a strong Couette flow. Even if $\tau = 0.5\tau_o$, $\ell \doteq 1.05\ \ell_c$, and for $\tau = 0.2\tau_o$, $\ell \doteq 1.12\ \ell_c$. This bears out the statement that the subject assumption is tantamount to the assumption of a "universal mixing length distribution," where $L^+ = f(Y^+)$, and both L^+ and Y^+ are based upon τ_o rather than τ.

PRESSURE PROFILES

Pressures in the large scale turbulence apparatus range upward to the magnitude of

$$p/\rho u_b^2 \doteq 3\times 10^{-3} \tag{17}$$

Since the "velocity pressure" is $\rho u_b^2/2$, even a one-percent change in velocity would create a pressure increment such that

$$\Delta p/\rho u_b^2 = 10^{-2} \tag{18}$$

Thus even a very small disturbance can create pressure changes that mask the true pressure. As a consequence of this delicacy of measurement, a great many runs were required to establish confident data. The end result showed a gratifying consistency, as indicated in Figures 9 and 10. In Figure 9, the time-readings in the pressure measurement instrument are shown, thus indicating a considerable variation in actual pressure from run to run. In Figure 10, the dimensionless pressure is plotted for the three runs and is seen to correspond well within expected experimental scatter despite the change in Reynolds number from run to run. These data will be analyzed further in the forthcoming period. As they stand, they confirm the general magnitude of the previous report, and thus sustain the previous arguments that both circumferential and axial flow are significant even in our short-bearing experimental setup ($L/D \doteq 1/3$).

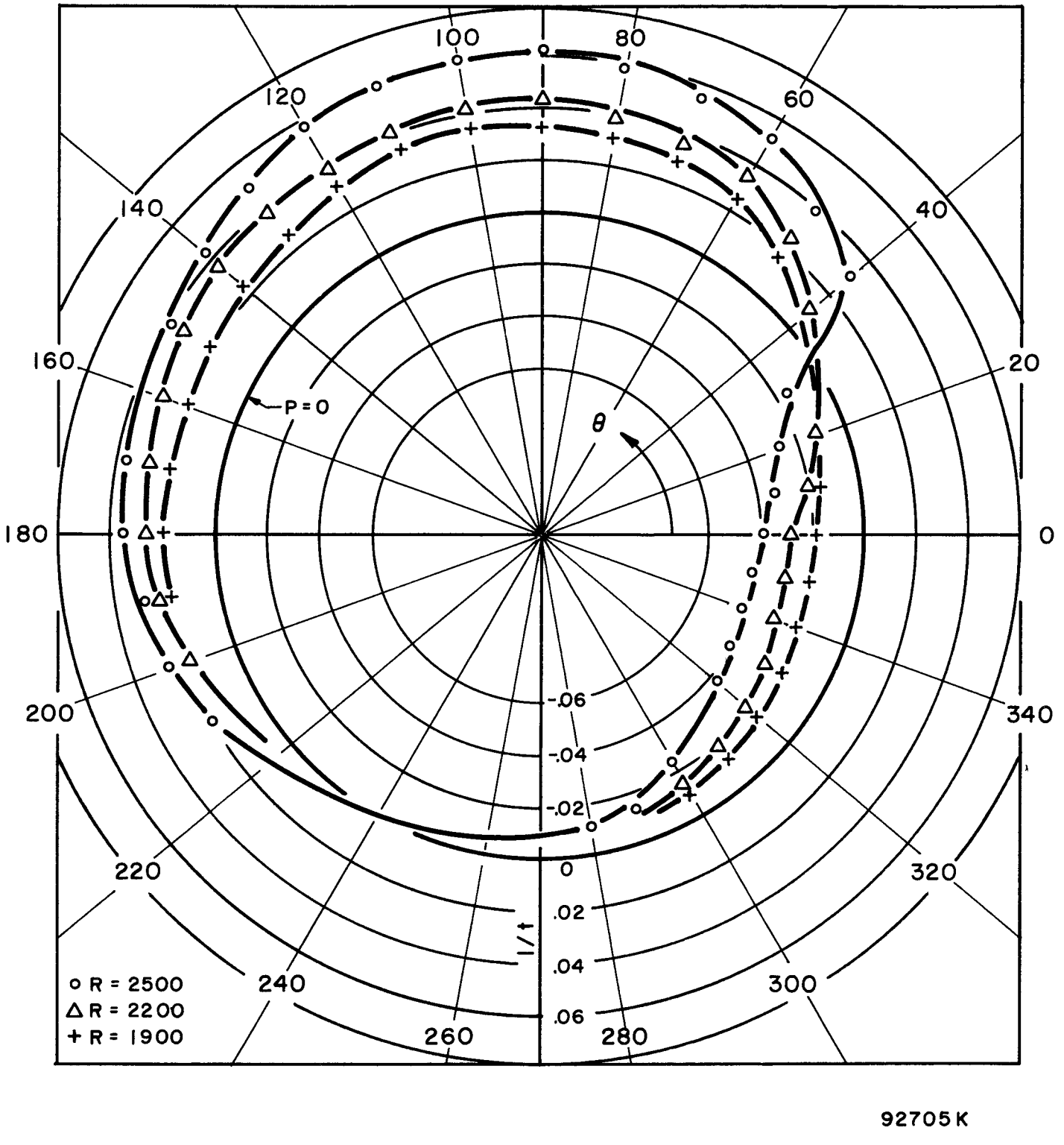

FIGURE 9. PRESSURE INSTRUMENT READINGS VS ANGULAR POSITION AROUND LARGE-SCALE TURBULENCE APPARATUS

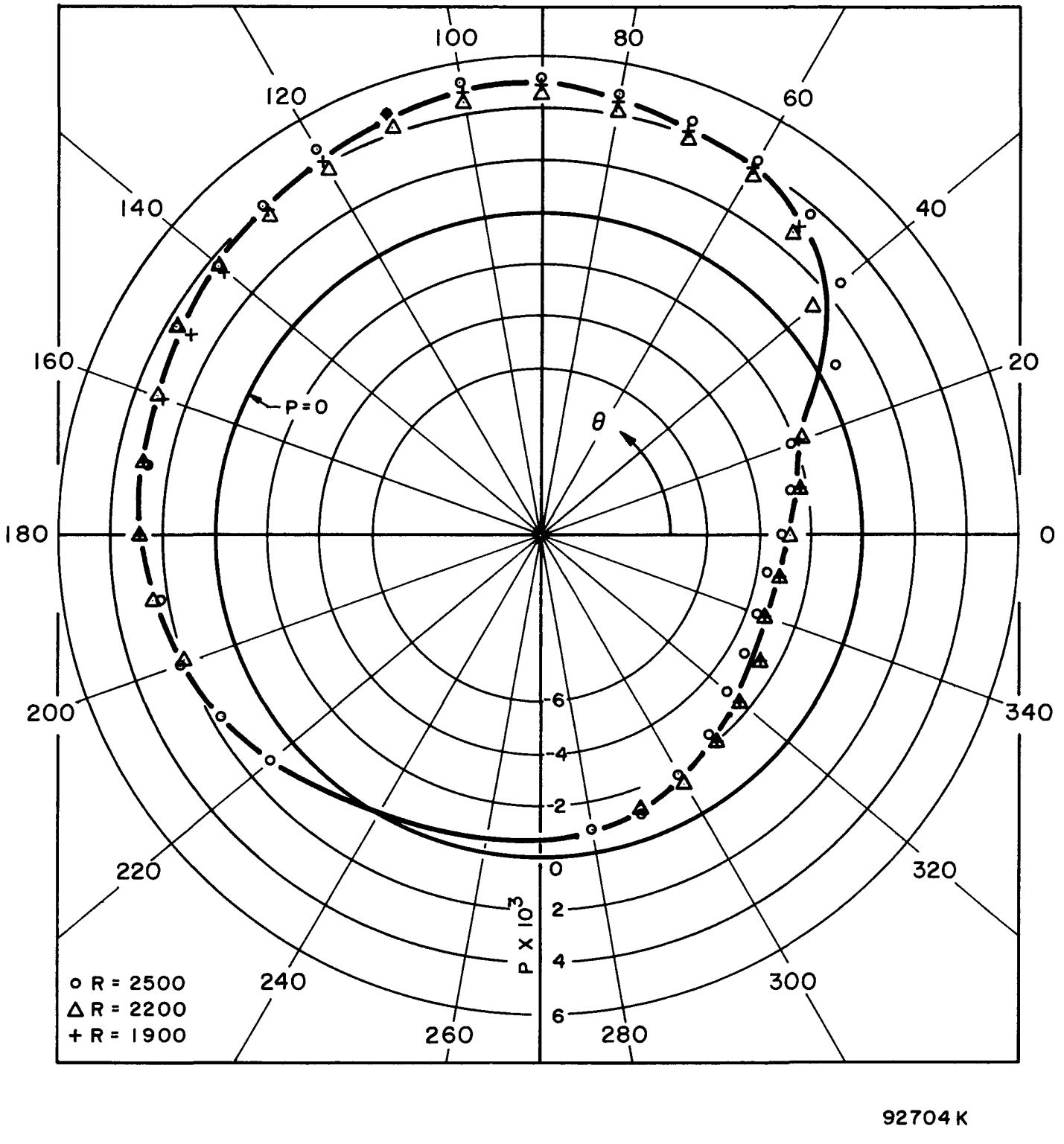

FIGURE 10. DIMENSIONLESS PRESSURE VS ANGULAR POSITION AROUND LARGE-SCALE TURBULENCE APPARATUS

SKEWED FLOWS

In operating the large-scale turbulence apparatus as a bearing, it was found that (even at large eccentricity) insufficient leakage flow would arise to permit a critical set of measurements on skewed flows. As an expedient approach, the "bearing" was placed concentric with the journal and an axial blockage was clamped to the bearing, in the form of a 0.5 in. $\times$ 0.5 in. board. This forced the flow to divert and pass out the ends of the clearance space, as fluid was transported to the barrier by traction on the moving journal. Two sets of data at two Reynolds numbers are reported here. Analysis of these data involves the complete solution for bearings with end leakage and will be attempted in the forthcoming quarter. At present these data are reported for their direct interest value.

Figure 11 shows a map of the local velocity vectors near the obstacle at low Reynolds number (R = 550). Here Z is measured from midchannel outward toward the edge in inches; X is measured from the barrier in inches. Note that the midstream velocity simply decelerates. Outward from this line the velocity turns into the axial direction and increases in magnitude.

Figure 12 shows a comparable figure at higher speed (R = 2500) where the pattern of flow is shifted somewhat - presumably due to inertial effects.

Figure 13 shows typical measurements of velocity-direction at a given (X, Z) point and for different values of y/b, at R = 2500.

Table 1 gives a series of pressure measurements which accompany the velocity pattern of Figure 12.

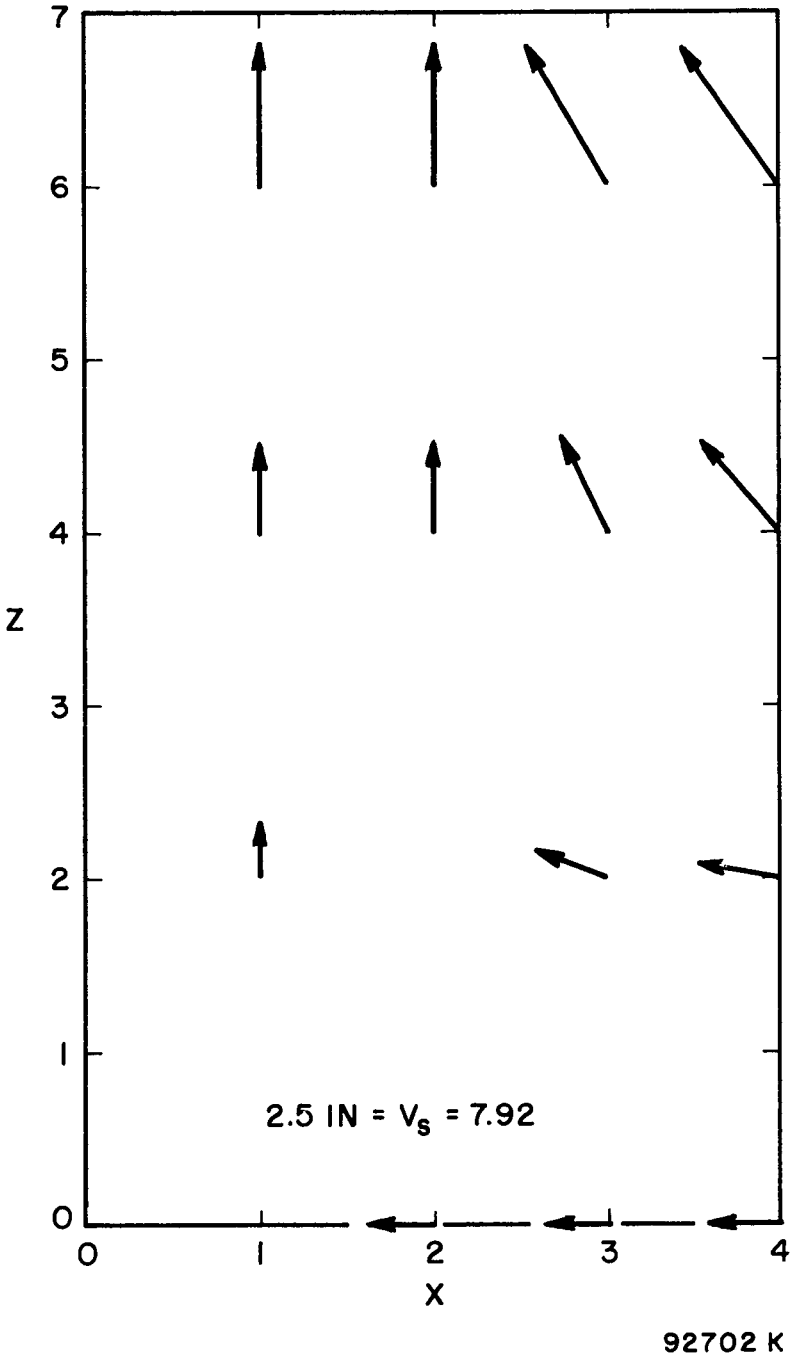

FIGURE 11. VELOCITY VECTORS IN SKEWED FLOW (R = 550)

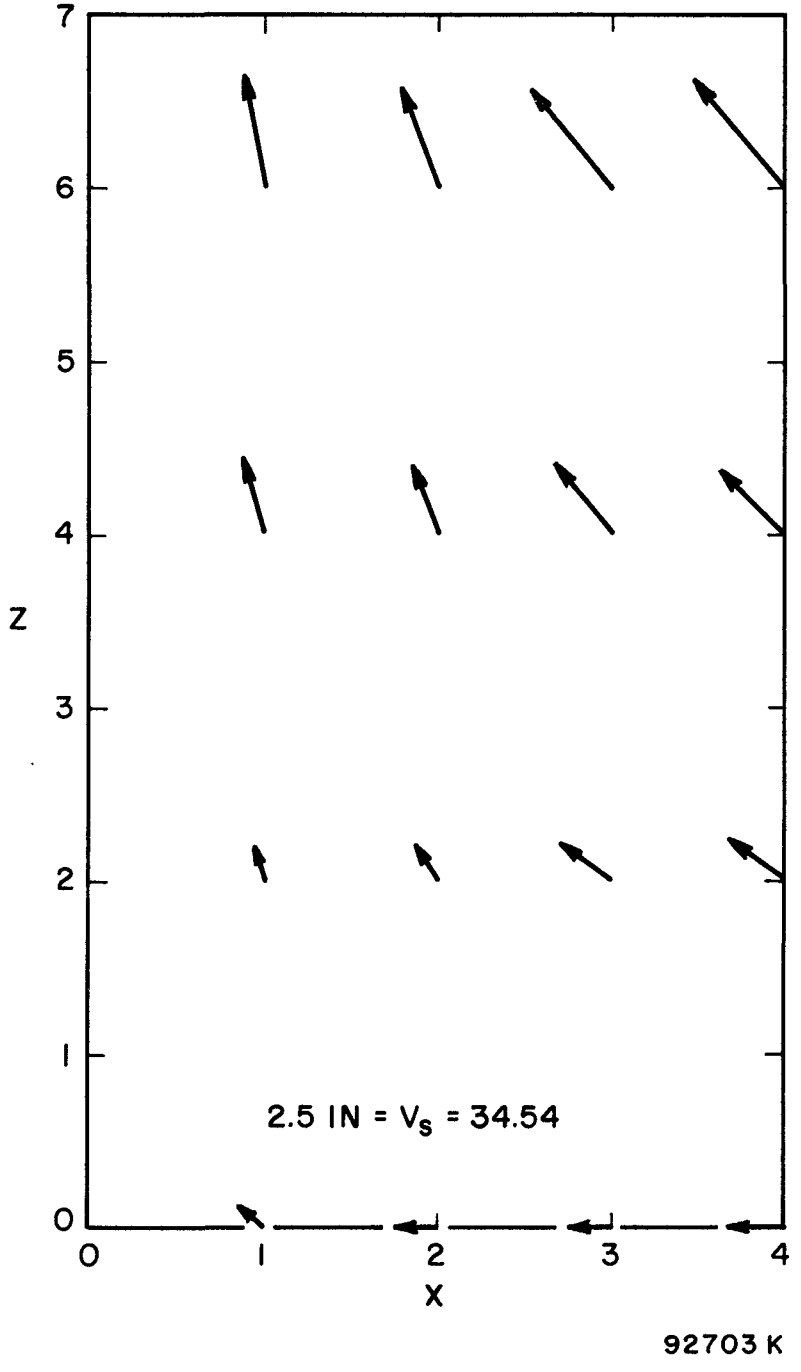

FIGURE 12. VELOCITY VECTORS IN SKEWED FLOW (R = 2500)

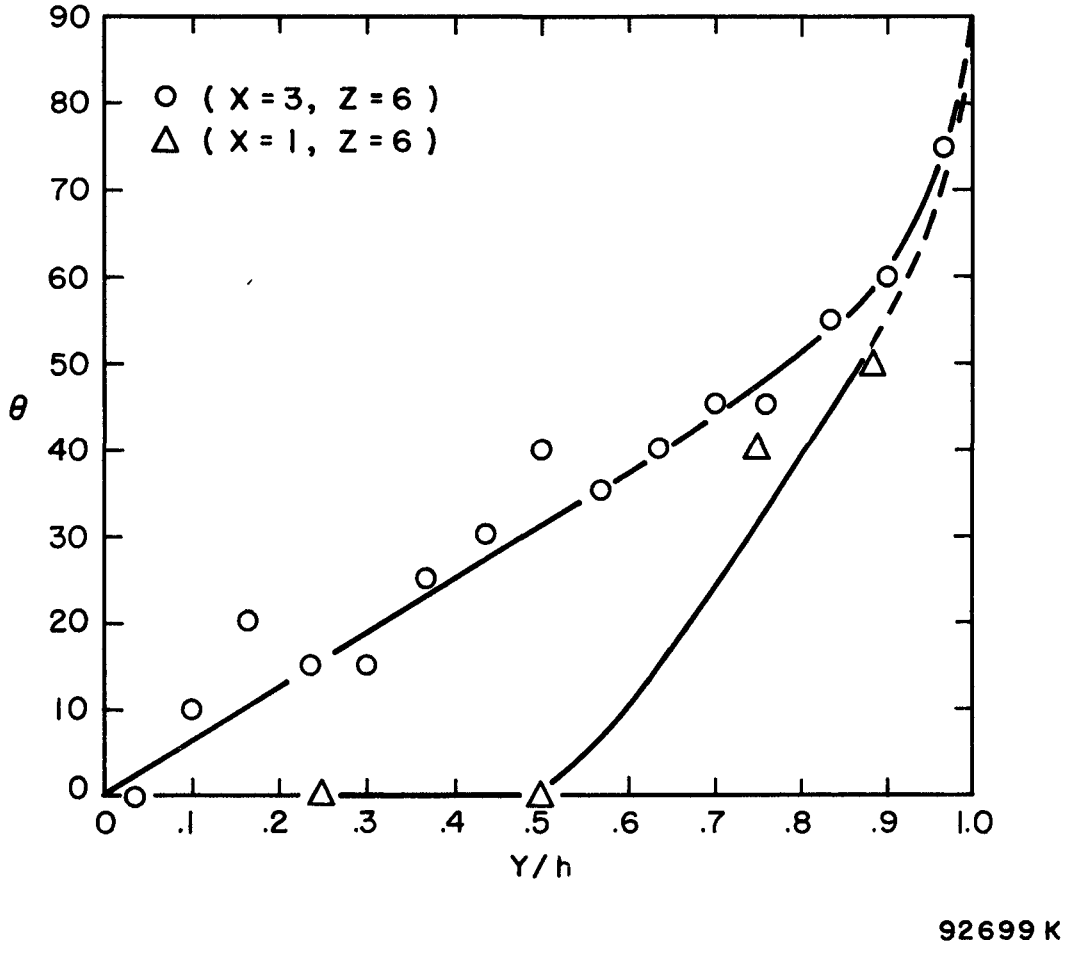

FIGURE 13. ANGLE OF VELOCITY VECTOR VS DIMENSIONLESS WALL DISTANCE (R = 2500)

TABLE 1. PRESSURE DISTRIBUTION IN SKEWED FLOW (R = 2500)

X, in.	Z, in.	P
1	0	0.374
	2	0.361
	4	0.337
	6	0.273
2	0	0.344
	2	0.337
3	0	0.321
	4	0.281
	6	0.220
4	0	0.297
	2	0.297
5	0	0.280
	4	0.253
	6	0.198

INERTIAL EFFECT ON A PAD WITHOUT END LEAKAGE AND WITH TURBULENT FLOW

Appendix A reviews the derivation of the equation for flow in a bearing without end leakage, showing it to reduce to the following form

$$-\frac{dP}{dX} = \frac{\zeta}{\chi^2}\frac{d\left(\frac{1-H}{H}\right)}{dX} + 2C_f\frac{\xi}{\chi}\left(\frac{1-H}{H^2}\right) \tag{19}$$

Letting $C_f' = C_f\frac{\xi}{\chi}$, this simplifies to

$$-\frac{dP}{dX} = \frac{-\zeta}{\chi^2}\frac{dH/dx}{H^2} + 2C_f'\left(\frac{1-H}{H^2}\right) \tag{20}$$

For an inclined flat slider on a flat surface

$$H = 1 - aX$$

$$\frac{dH}{dX} = -a$$

Substituting this into Eq. (20)

$$\frac{dP}{dX} = \frac{\zeta}{\chi^2}\frac{a}{(1-aX)^2} + \frac{2C_f'}{A}\left(\frac{a}{(1-aX^2)} - \frac{a}{(1-aX)}\right) \tag{21}$$

Letting $Q \equiv (1 - aX)$

$$\frac{dP}{dX} = \frac{-\zeta}{\chi^2}\frac{dQ}{Q^2} + \frac{2C_f'}{a}\left[-\frac{dQ}{Q^2} + \frac{dQ}{Q}\right] \tag{22}$$

If it is assumed, as outlined in Appendix A, that ζ/χ^2 and C_f' may be dealt with approximately as constants

$$-P = \frac{\zeta/\chi^2 + 2C_f'/a}{(1-aX)} + \frac{2C_f'}{a}h(1-aX) + N \tag{23}$$

Under the same simplifying assumption, P may be integrated a second time; however, Eq. (23) was considered to be sufficiently simple for numerical integration.

To evaluate the constant of integration N, the leading edge pressure must be assumed. The full span of possibilities can be covered by three choices: (1) The value of N = 0 would correspond to the absence of inertial effect, (2) The value of N = 2 would correspond to full stagnation pressure at the entry. The value of N = 1 would correspond to recovery of half the stagnation pressure at entry -- and, pending experimental verification, might represent a logical magnitude.

Summarizing all of the combinations of variables chosen

N	ζ/χ	c_f	a	X_o
0	0	0.005	0.001	-200 -400 -800
0	0	0.005	0.005	-100 -200 -400
0	0	0.005	0.01	- 20 - 40 - 80
2	1	0.005	0.001	-200 -400 -800
2	1	0.005	0.005	-100 -200 -400
2	1	0.005	0.01	- 20 - 40 - 80
1	1	0.005	0.001	-200 -400 -800
1	1	0.005	0.005	-100 -200 -400
1	1	0.005	0.01	- 20 - 40 - 80

The choices of N have been explained above. The choice of $\zeta/\chi = 0$ simply eliminates the inertial term from Eq. (19). C_f represents a plausible magnitude from the previously shown C_f charts and the magnetudes of ζ/χ^2

as indicated in Appendix A. The slope a provides bearings with a clearance/length ratio ranging roughly from 0.0005 to 0.05; this would imply for 0.001 in. central clearance that pads would range from 2 in. down to 0.2 in. Thus, a plausible range of conditions has been covered. The quantity X_o measures the position of the pad's leading edge from an arbitrary point, where H is assigned a value of unity. This arbitrary point corresponds approximately to the mean film thickness.

Computer Results

A. Pressure Profiles. Figures 14 thru 16 show three sets of pressure profiles, showing the effect of pad length L (expressed as a multiple of mean film thickness) and N (the pressure recovery factor). Because L was not one of the pre-set parameters in the program, exactly comparable values are not available for all of the magnitudes of N. On the other hand, they are sufficiently close to permit useful comparisons. The principal feature to note in these plots is that the leading-edge impact pressure N is a major factor in determining the pressure profile. Figures 15 and 16 show similar relations for different pad angles.

B. Location of Center of Pressure. In Figure 17, the symbol $\bar{C}/L$ represents the distance back from the leading edge to the center of pressure, expressed as a fraction of pad length. The subscript on $\bar{C}_N$ corresponds to the magnitude of N used in the calculation. Note that for N = 0 (i.e., no impact pressure), the center of pressure is behind the pad center, as is true in laminar flow. For N = 1, the center of pressure is well ahead of

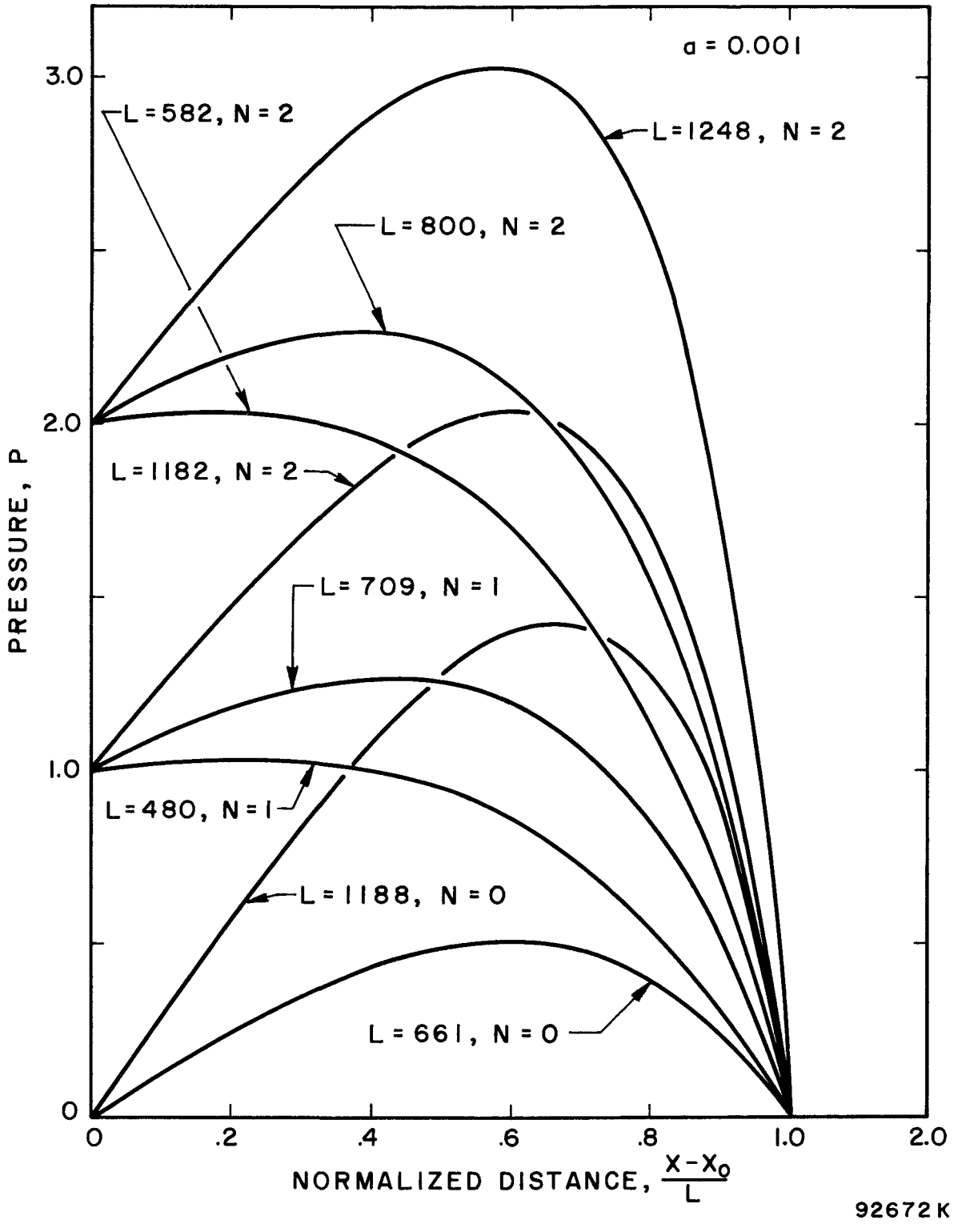

FIGURE 14. PRESSURE DISTRIBUTIONS UNDER TILTED PAD FOR a = 0.001

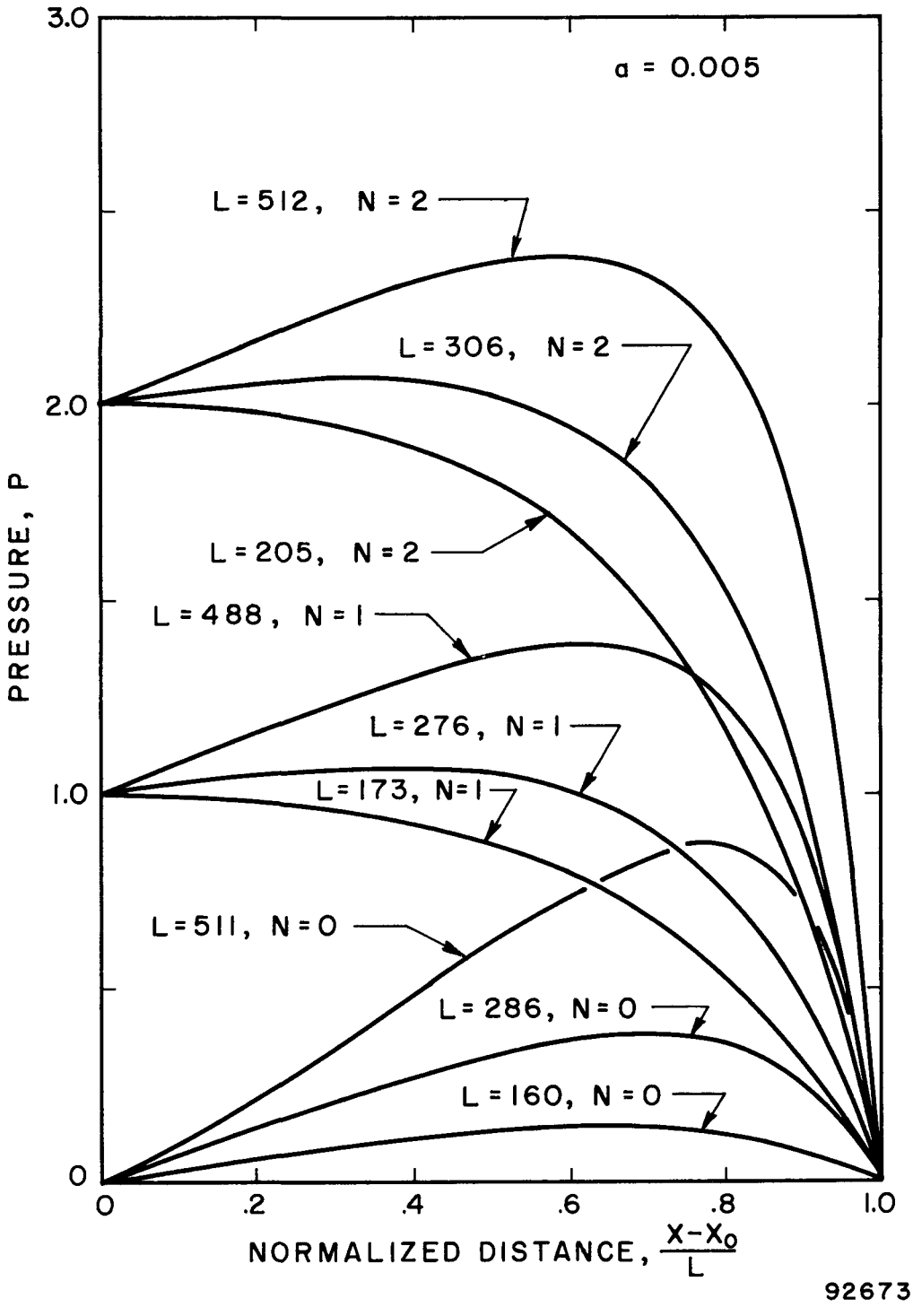

FIGURE 15. PRESSURE DISTRIBUTIONS UNDER TILTED PAD FOR a = 0.005

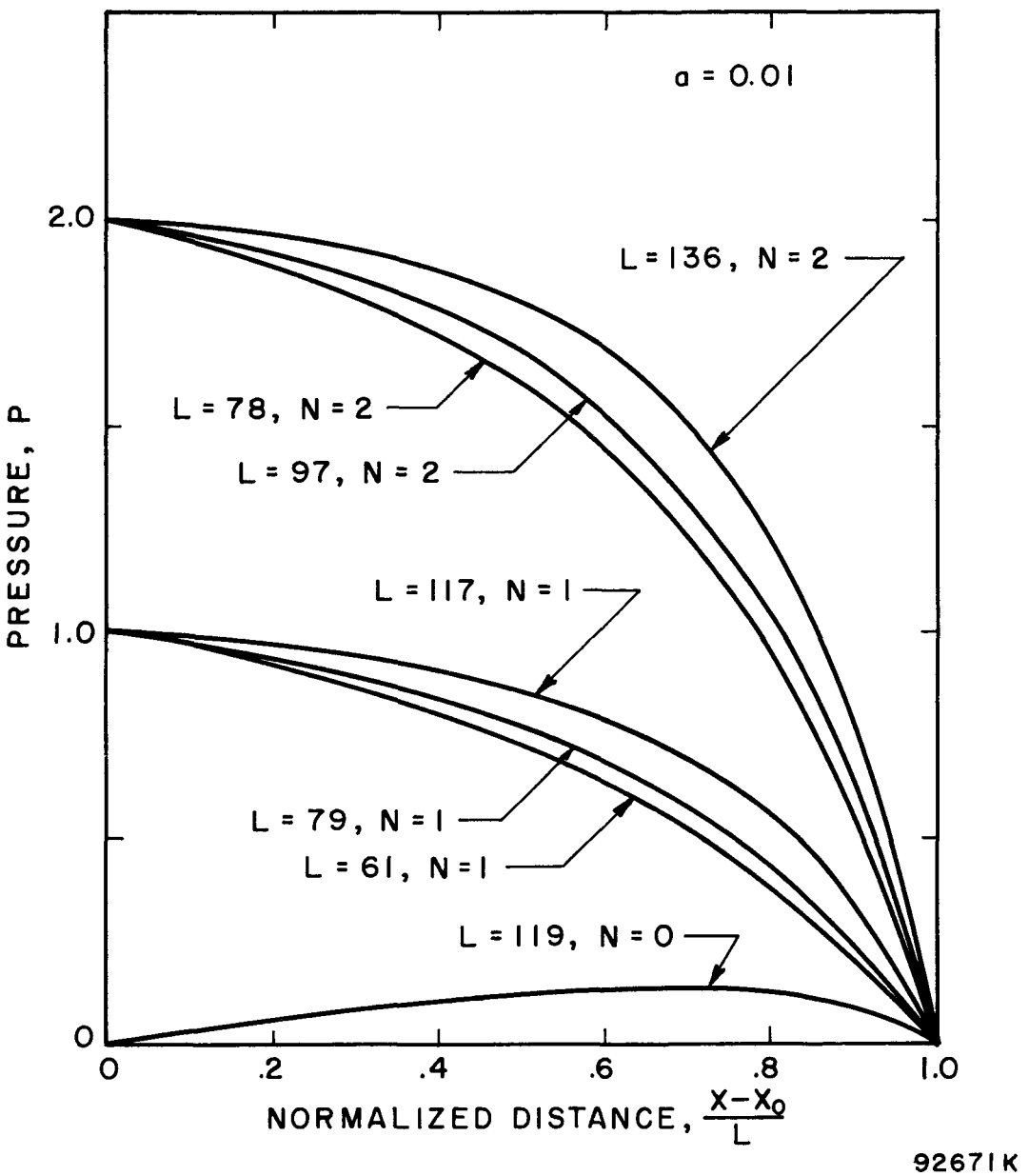

FIGURE 16. PRESSURE DISTRIBUTIONS UNDER TILTED PAD FOR a = 0.010

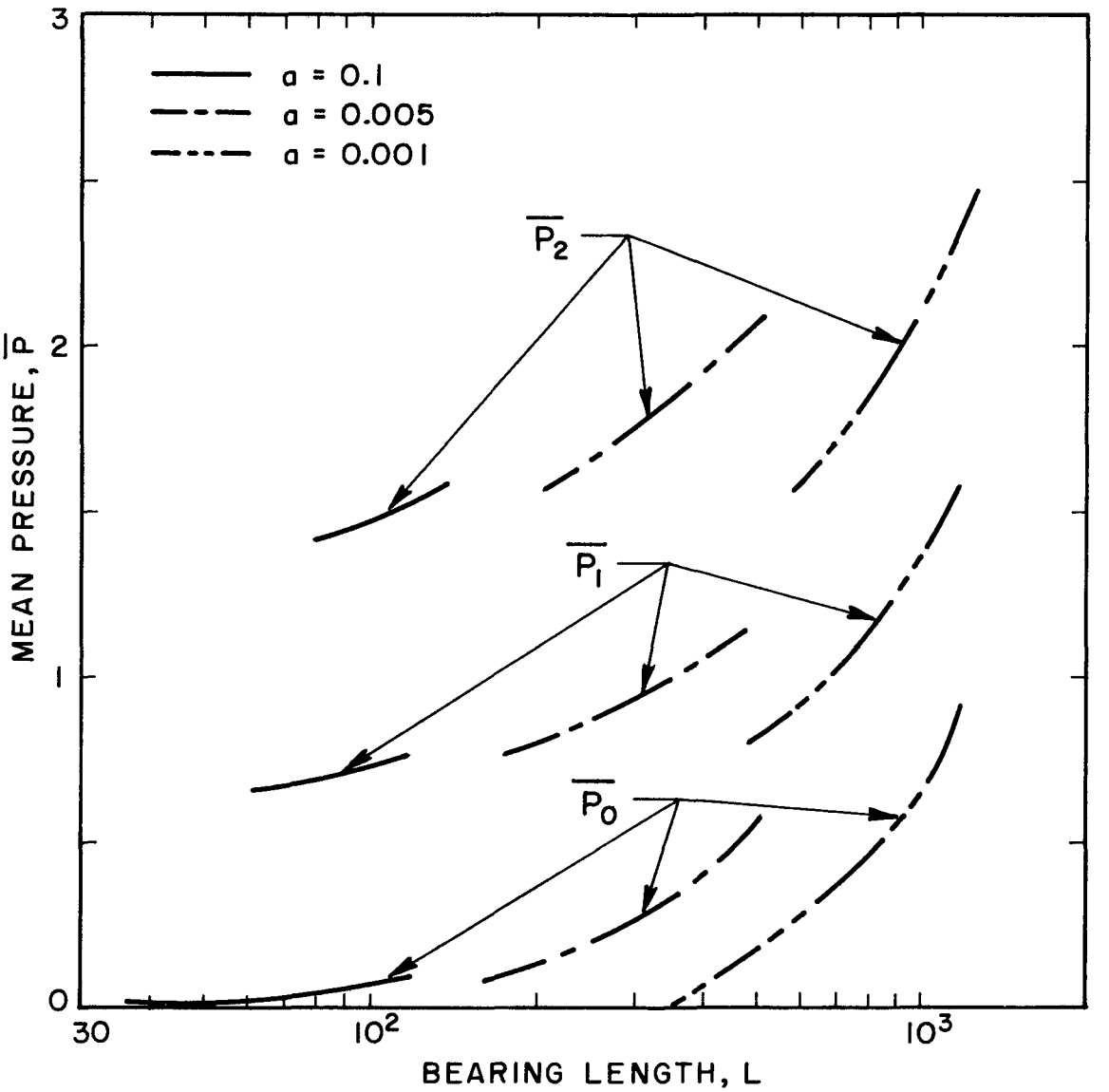

FIGURE 17. LOAD SUPPORT CHARACTERISTICS OF TILTED PAD

the center of the pad, moving backward for longer values of bearing length L. Note also that for increasing pad angle the center of pressure moves rearward. Thus, for a pivoted bearing there will be stability in the sense that, for a given pivot position, pad angle will increase until the center of pressure moves to the pivot position. One would conclude from the calculated values that pivot location at midpoint of the pad ($\bar{C}_N/L = 0.5$) is not unrealistic for turbulent-film bearings. It also suggests that if the pad is to be subject to either laminar or turbulent flow a pivot position near to the halfway point is desirable.

C. Load Carrying Capacity. The mean pressure $\bar{P}_N$ is plotted in Figure 18, where it is seen to be significantly affected by the impact pressure, as determined by N. Otherwise, it is shown to increase regularly with bearing length and with pad-angle as given by a. It is interesting that the principal effect of impact pressure is to elevate the complete family of curves. Surprisingly, the elevation is not the initial value of P (i.e., of N); it is smaller, running nearer to 0.75 N. Perhaps this observation can be used as a rule of thumb for future calculations.

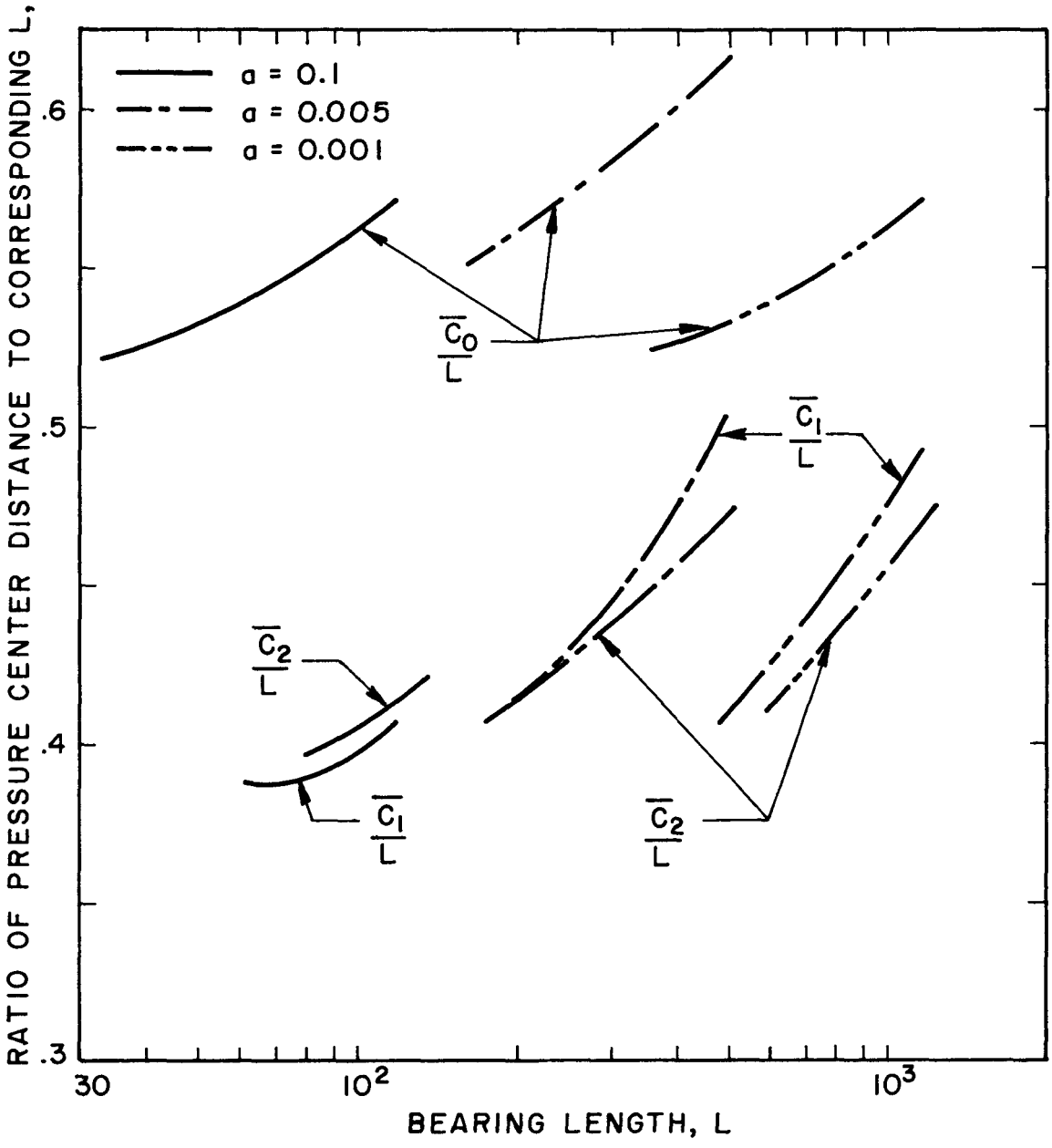

FIGURE 18. LOCATION OF CENTER OF PRESSURE FOR TURBULENT FLOW UNDER TILTED PAD

PHYSICAL CONCEPT OF LEADING-EDGE IMPACT PRESSURE RISE

Refering to Figure 19, visualize the shaft surface as moving to the right (with the speed u_s), and drawing with it boundary-layer fluid at the same speed. At entry to the bearing, the mean fluid velocity must achieve the ultimate value of u_b (at the extreme right), thus continuity considerations dictate that a sizeable part of the flow must be deflected. One might visualize an entry as shown, corresponding to orifice flow with a vena contracta, by a "dead water" region and followed by a mixing zone. If the velocity at the vena contracta is still u_s then $u_s h_a = u_b h$. The momentum flux equation between a and b may be written approximately as

$$hp_a + (\rho u_s h_a)u_s \doteq hp_b + (\rho u_b h)u_b \tag{24}$$

or

$$p_b - p_a \doteq \rho\, u_b h(u_s - u_b) \tag{25}$$

If $u_b \doteq \frac{1}{2}\, u_s$

$$p_b - p_a \doteq \rho u_b^2 \tag{26}$$

or

$$\frac{\Delta p}{\rho u_b^2} \doteq 1 \tag{27}$$

One factor which would lower this magnitude would be prior dissipation in the region of deceleration which must precede entry to the bearing. In that region there must be a pressure rise to deflect the flow and consequently

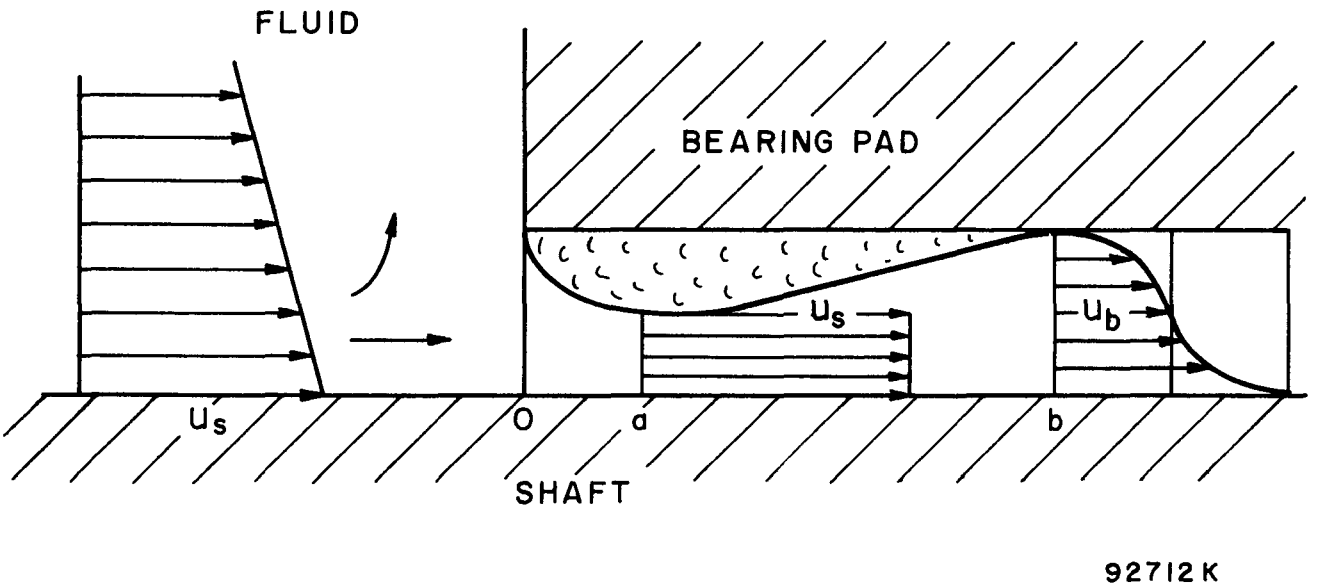

FIGURE 19. ILLUSTRATION OF FLOW AT ENTRANCE TO TILTED PAD

the fluid must move into an "adverse pressure gradient" with attendant deceleration--and possibly with separation and the losses which accompany this. Only experimental measurements will answer this question completely.

FUTURE PROGRAM

The principal effort of the forthcoming quarter will be to round out and exploit further the findings and methods of analysis indicated in this report. It was noted in the previous report that the subject of combined pressure-flow and Couette-flow would be dealt with in the vortex-flow regime, in the present report. However, during the preparation period, a paper has been published by Di Prima on this subject[9]. It is felt appropriate to hold discussion of this subject back until this recent work has been assessed.

REFERENCES

1. Miles, J. W., "On the Velocity Profile for Turbulent Flow Near a Smooth Wall," Journal of the Aeronautical Sciences, 24, Sept. 1957, p. 704

2. van Driest, E.R., "On Turbulent Flow Near a Wall," Journal of the Aeronautical Sciences, 23, No. 11, Nov. 1956, pp. 1007-1011.

3. Szablewski, W., "Berechnung der turbulenten Stromung in Rohr auf der Grundlage der Mischungsweghypothese," Z. Angew. Math. and Mech., 31, No. 4/5, April/May, 1951, pp. 131, 138.

4. Reichardt, H., "Vollstandige Darstellung der Turbulenten Geschwindigheitsverteilung in glatten Leitungen," Z. Angew. Math. and Mech., 31, No. 7, July 1951, pp. 208-214.

5. Ng, C.W. and Pan, C.H.T., "A Linearized Turbulent Lubrication Theory," Paper, International Lubrication Conference, Oct. 1964.

6. Schlichting, H., Boundary Layer Theory, McGraw Hill Book Co., Inc., New York, 1960, p. 505

7. Emmons, H.W., "Shear Flow Turbulence," Proc. Nat. Cong. Appl. Mech., 2nd, ASME, 1954, pp. 1-12.

8. Di Prima, R.C., "Viscous Flow Between Rotating Concentric Cylinders with a Circumferential Pressure Gradient at Speeds Above Critical," ASLE Trans., 7, No. 4, October, 1964, pp. 333-341.

APPENDIX A

In Progress Report No. 2 equations were outlined for bearing analysis. The derivations presented at that time have been improved and corrected here, preparatory for ultimate incorporation into a more general derivation for flow with end leakage.

The ultimate goal of the present derivation is to generate an equation for circumferential flow, of the type:

$$\zeta(1 + U)\frac{\partial U}{\partial X} + 2C_f\xi\frac{U}{H} = -\frac{dP}{dX} \tag{1}$$

where

$$\frac{\Delta u_b}{u_{bc}} \equiv U,\ x/h_o \equiv X,\ h/h_o \equiv H,\ p/\rho u_{bc}^2 \equiv P,\ C_{fc} \equiv C_f,\ R = r/h_o$$

and

$$\xi \equiv \frac{C_{fo}(u_{bc} + \Delta u_b)^2 - C_{fh}(u_{bc} - \Delta u_b)^2}{4C_{fc}(u_{bc})\Delta u_b} \tag{2}$$

$$\chi \equiv \frac{\int_0^h \Delta u\, dy}{\Delta u_b h} \tag{3}$$

$$\zeta \equiv \frac{\int_0^h (u_c + \Delta u)\frac{\partial \Delta u}{\partial x}\, dy}{2bu_{bc}\left(1 + \frac{\Delta u_b}{u_{bc}}\right)\frac{\partial \Delta u_b}{\partial x}} \tag{4}$$

The last three quantities are shown to be weak variables and, of the order of unity.

present case, these need not be discussed here. An expression of Newton's second law for such a film* may be written as follows (under the assumption of steady flow with the local velocity u in the x direction, and where pressure is assumed to be independent of y, the coordinate measured across the film thickness, which ranges from 0 to h):

$$\int_0^h \rho u \frac{\partial u}{\partial x} dy + \frac{\partial p}{\partial x} h = \tau_h - \tau_o \tag{5}$$

It is now possible to introduce the definition

$$C_f = \frac{2|\tau|}{\rho u_b^2} \tag{6}$$

such that C_f is defined relative to the wall on which the shear stress is to be measured, and u_b is defined as midchannel velocity relative to that wall. Substituting into Eq. (4)

$$\int_0^h \rho u \frac{\partial u}{\partial x} dy + \frac{\partial p}{\partial x} h = \left[\frac{C_{fh}\, \rho (u_{bh})^2}{2}\right]_h - \left[\frac{C_{fo}\, \rho (u_{bo})^2}{2}\right] \tag{7}$$

Refer to Figure 1-A for which the definition of the relative velocities u_{bh} and u_{bo} are defined.

At this point it is desirable to refine further the definition of u_b in order to examine the case of a pressure flow, acting codirectional with a Couette flow. As illustrated in Figure 1-B, a Couette flow with centerline velocity u_{bc} is incremented to the right by a pressure flow, where the incrementation of the centerline velocity is of the magnitude Δu_b.

*For turbulent or laminar film.

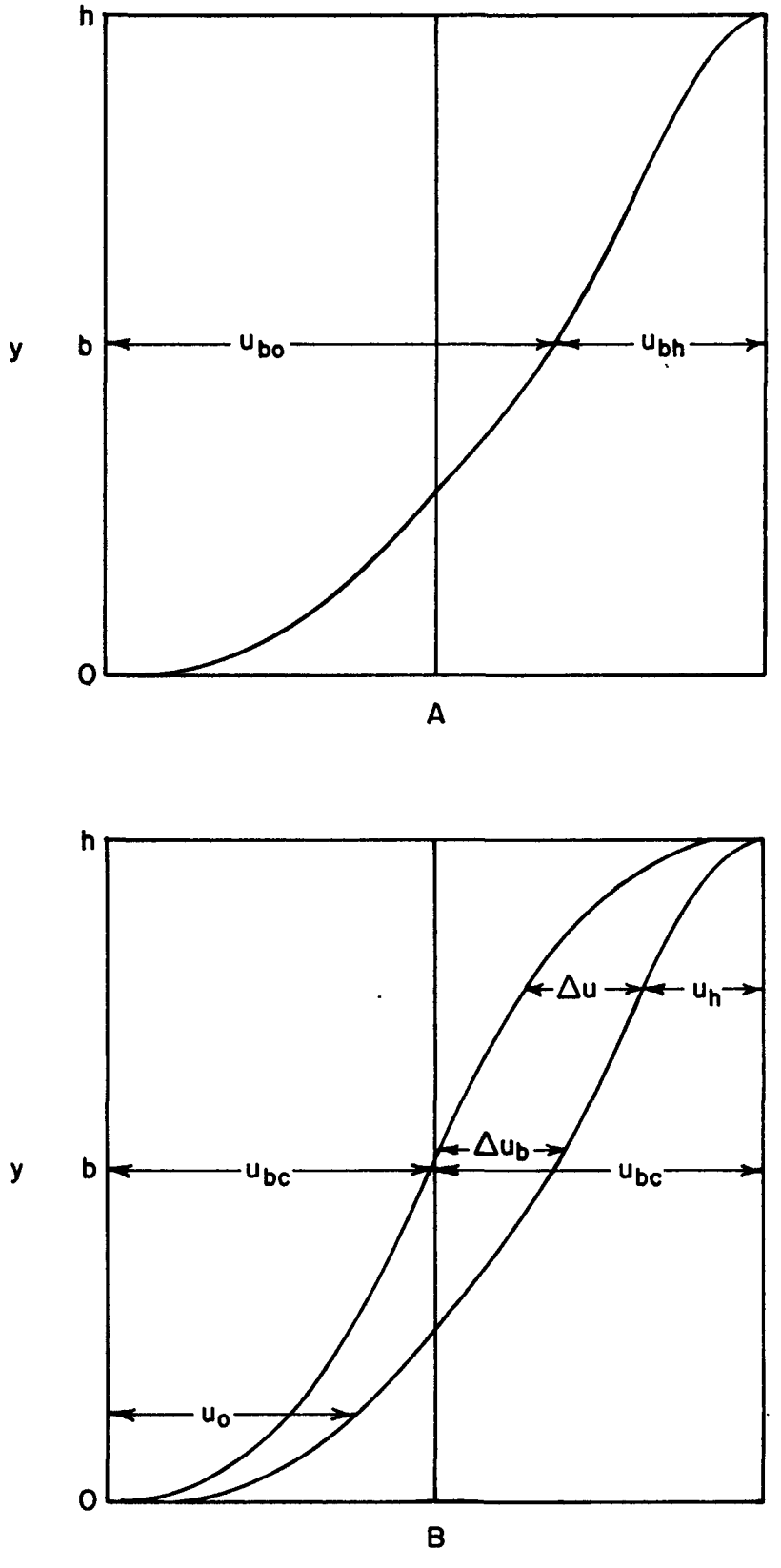

FIGURE 1. NOMENCLATURE FOR ANALYSIS OF BEARINGS WITHOUT END LEAKAGE

In view of the definitions of u_{bo} and u_{bh}, these become

$$|u_{bo}| = |u_{bc} + \Delta u_b|$$

$$|u_{bh}| = |u_{bc} - \Delta u_b|$$

Here it is recognized that the Couette flow bears such symmetry relative to each wall that the mid-channel velocity is, in either case, designated by the same quantity u_{bc}, relative to either wall, for the Couette flow acting alone. In terms of this, Equation (6) becomes

$$\underbrace{\int_0^h \rho u \frac{\partial u}{\partial x} dy}_{\text{I}} + \underbrace{\frac{\partial p}{\partial x} h}_{\text{II}} = \underbrace{\frac{C_{fh}\rho(u_c - \Delta u_b)^2}{2} - \frac{C_{fo}\rho(u_c - \Delta u_b)^2}{2}}_{\text{III}} = 0 \quad (8)$$

The equation has been divided into three parts for purposes of discussion, part I being the "momentum flux" term, part II being the "pressure gradient" and part III being the "wall shear" term.

2. Wall Shear Term

If C_{fc} is the wall shear stress for the Couette flow before its incrementation by Δu, it is possible to write for other conditions the relation

$$\phi = \frac{C_f}{C_{fc}} \quad (9)$$

Hence ϕC_{fc} will permit the computation of actual friction coefficient C_f when ϕ is known. To obtain some idea of the type of variation expected of ϕ we may write the approximate expression:

$$\phi = \frac{C_f}{C_{fc}} = \left(\frac{R_c}{R}\right)^n \tag{10}$$

In this case we have assumed that the C_f vs R relationship is continuous and can be approximated by suitable selection of n. This would not necessarily be the same n that would best represent the Reynolds number variation for the Couette flow alone, though evidence has been presented (see Progress Report No. 1) which suggests that n will not differ greatly from that magnitude. In terms of this, Term III of Equation (8) becomes

$$(III) = \rho C_{fc}\left(\frac{u_{bc}}{u_{bc}+\Delta u_b}\right)^n \frac{(u_{bc}+\Delta u_b)^2}{2} - \rho C_{fc}\left(\frac{u_{bc}}{u_{bc}-\Delta u_b}\right)^n \frac{(u_{bc}-\Delta u)}{2} \tag{11}$$

Or using Equation (10)

$$(III) = \rho \frac{C_{fc}u_{bc}^2}{2}\left[\left(1+\frac{\Delta u_b}{u_{bc}}\right)^{2-n} - \left(1-\frac{\Delta u_b}{u_{bc}}\right)^{2-n}\right] \tag{12}$$

If n = 0 (in which case $C_f = C_{fc}$ = Const.), Equation (12) would reduce to

$$(III) = \rho \frac{C_{fc}u_{bc}^2}{2}\left[\frac{4\Delta u_b}{u_{bc}}\right] \tag{13}$$

This would be expected to prevail where wall roughness causes C_f to depart from smooth-wall behavior and level out at a nearly constant value at high Reynolds number.

Using the results of Equation (13) and Equation (12), a useful comparison is the consequence when the following quotient is determined:

$$\xi = \frac{\left[\left(1 + \frac{\Delta u_b}{u_{bc}}\right)^{2-n} - \left(1 - \frac{\Delta u_b}{u_{bc}}\right)^{2-n}\right]}{4(\Delta u_b/u_{bc})} \tag{14}$$

The quantity ξ would compare the effect of C_f varying, with that of constant C_f as to their influence on term III. Table II shows comparisons of the variation of ξ with $\Delta u_b/u_{bc}$ for $n = 1/2$ and $n = 1/4$, which would be expected to represent a realistic range of magnitudes.

Table II

	ξ	
	$n = 1/2$	$n = 1/4$
$\Delta u_b/u_{bc} \to 0$	0.75	0.875
$\Delta u_b/u_{bc} = \pm 1/2$	0.741	0.866
$\Delta u_b/u_{bc} = \pm 1$	0.70	0.84

Note that for $\Delta u_b/u_{bc} \to 0$, $\xi \to 1 - \frac{n}{2}$. Also note that $\Delta u_b/u_{bc} = 1$, represents the limit of applicability of Equation (8), as written, since exceeding of this magnitude would require a change of the sign in Term III of Equation (8), since the shear stress at one wall would reverse direction.

In terms of ξ, and Equation (12), Term III becomes

$$(III) = \rho \frac{C_{fc} u_{bc}^2}{2} \xi \left[\frac{4\Delta u_b}{u_{bc}}\right] \tag{15}$$

In recognizing that $\rho C_{fc} u_{bc}^2/2$ is the wall shear stress τ_c of the original Couette flow acting alone

$$(III) = \tau_c \xi \left[\frac{4\Delta u_b}{u_{bc}}\right] \tag{16}$$

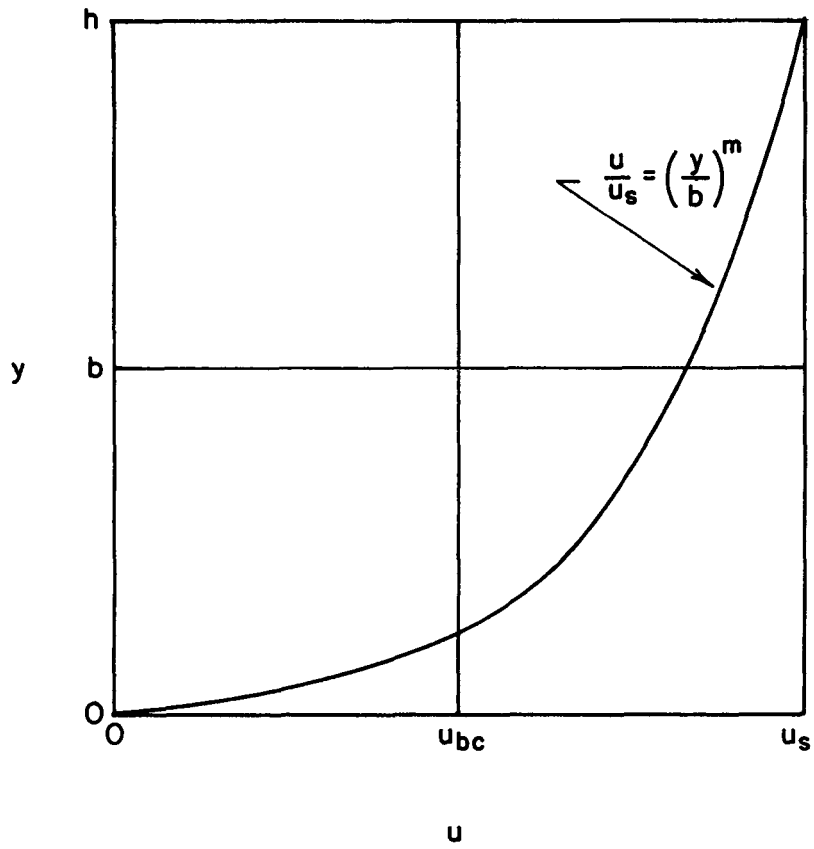

FIGURE 2. ILLUSTRATION OF APPROXIMATE VELOCITY PROFILE WHEN $(\Delta u_b)/u_{bc} \rightarrow 1$

This is a useful form of the term since ξ is not widely variable, as is seen in Table II. As a first approximation, it could well be $\xi = 1 - \frac{n}{2}$. If more accuracy is desired any reasonable choice of n will give a fair approximation since, for the wide range indicated, the ratio of ξ for the two values of n is about 0.85; or, only a 15% error in Term III would have resulted if one value of n had been used for computation when the other should apply. Somewhere between these extremes even better agreement should result.

Should we, in measurement, be able to determine n within 20% of its best value, only a very small error in Term III would result. This suggests the feasibility of obtaining realistic predictions of the "wall shear" term by reasonably accurate experimentation.

3. Momentum Flux

In Equation (8) the momentum flux term, Term I, may be written as

$$(I) = \frac{d\int_0^h \rho \frac{u^2}{2} dy}{dx} = \rho \frac{d\left[\left(\zeta \frac{\rho u_b^2}{2}\right)h\right]}{dx} \qquad (17)$$

A new dimensionless quantity ζ is introduced to account for the variation of u. It is of interest to determine the general magnitude of ζ and its sensitivity to the shape of the velocity profile. We note that

$$\zeta \equiv \frac{\int_0^h \frac{\partial u^2}{\partial x} dy}{h\frac{\partial \Delta u_b^2}{\partial x}} \qquad (18)$$

Though some additional analysis is possible, we shall proceed directly to an order-of-magnitude investigation of factors influencing the term by the assumption that both u_c and Δu vary out from a wall into either half channel according to an equation of the form $u/u_b = (y/b)^m$. In addition to approximating the flow in each half channel by a power-law profile, it assumes that the law is identical for each. In terms of this, Equation (17) becomes

$$\zeta h u_b^2 = \int_0^b (u_{cb} + \Delta u_b)^2 (y/b)^{2m} + \int_b^h [2u_{cb} - (u_{cb} - \Delta u_b)]^2 (y/b)^{2m} \tag{19}$$

To obtain some information on the variation of ζ, it is desirable to insert some numerical value of m, which for the present has been chosen as 1/7. In addition to ζ, two additional parameters have been included in the calculations, and these have been defined as follows

$$A \equiv \frac{\int_0^h u^2 dy}{u_{bc}^2 h} \tag{19}$$

$$B \equiv \frac{(u_{bc} + \Delta u_b)^2}{u_{bc}^2} \tag{20}$$

and

$$A/B = \zeta \tag{21}$$

Table III compares A, B and ζ for different values of $\Delta u_b/u_{bc}$.

Table III

$\Delta u_b/u_{bc}$	A	B	ζ
0	1.006	1	1.006
+1	3.789	4	.947
-1	0.012	0	∞

Note that though $\zeta = \infty$ for $\Delta u_b/u_{bc} \rightarrow -1$, this is not to be misinterpreted as making ζ a useless parameter. Comparison of A and B shows that the momentum flux prediction using the approximate profile, follows the simple prediction reasonably well. Thus if ζ were assumed to be unity and applied to B, it would predict A = 0 rather than the very small value of 0.012, computed by the more accurate estimate of the profile.

4. Continuity

The continuity equation for an incompressible lubricant film may be written as follows:

$$(h_o - h)\, u_{bc} = \int_0^h \Delta u \; dy \tag{22}$$

Here there is no normal motion between surfaces, and h_o is film thickness where only Couette flow would prevail. It may, in fact, be a hypothetical thickness which does not exist in a bearing, but nevertheless serves as a parameter to characterize the flow.

To determine how the integral $\int_0^h \Delta u \, dy$ is influenced by velocity profile form, let us use, as previously, a profile in the half channel (for velocity relative to the nether wall) $\Delta u/\Delta u_b = (y/b)^m$. Equation (22) becomes

$$(h_o - h)u_{bc} = 2 \int_0^b \Delta u_b (y/b)^m \, dy$$

or integrating

$$(h_o - h)u_{bc} = \frac{2\Delta u_b b}{m+1} = \frac{\Delta u_b h}{m+1} \tag{23}$$

Had the velocity Δu_b prevailed across the channel as a "constant" increment to the flow the result would have been

$$(h_o - h)u_{bc} = \Delta u_b h \tag{24}$$

The ratio of the right-hand term in Equation (23) to the equivalent term in Equation (24) may be designated by χ and would be, for $m = 1/7$,

$$\chi = \frac{1}{m+1} = 0.875 \tag{25}$$

Again the critical quantity is close to unity. Hence the correction due to the choice of m tends not to be a major factor. Irrespective of the particular value of m, the continuity equation written in the following form must be correct:

$$(h_o - h)u_{bc} = \chi \Delta u_b h \tag{26}$$

5. Extreme Conditions

It has been mentioned that the preceding analysis cannot be applied without alteration outside the range $-1 < \Delta u_b/u_{bc} < +1$. Furthermore, the approximate power law expressions for C_f and velocity profile must breakdown where $\frac{u_{bc} - \Delta u_b}{u_{bc}} \to 0$. On the other hand, shear stress tends also to go to zero in this case, which makes the precise magnitude relatively unimportant.

To show how insensitive a typical quantity might be to gross departures of velocity profile from the chosen form, let us examine the somewhat more realistic power law profile approximation shown in Figure 2, with respect to the continuity equation.

$$(h_o - h)\, u_c = \int_0^h \Delta u \, dy = \int_0^h \frac{2u_{bc}}{h^m} y^m dy - u_{bc}h = \frac{zu_{bc}h}{m+1} - u_{bc}h$$

$$= \frac{(1-m)u_{bc}h}{m+1} \tag{27}$$

When Eq. (27) is compared with Eq. (26), we note that

$$\chi = \frac{1 - m}{(m + 1)} \tag{28}$$

If, for instance, $m = 1/7$, $\chi = 0.75$, which is not greatly different from the value of 0.875 given by the previous computation in Equation (25).

6. Summary

Though additional comparisons can be made, it is futile to do so without further knowledge of actual velocity profiles. There is nevertheless reassurance in the observation that ζ, ξ and χ are all near unity and are all relatively insensitive to the details of the velocity profile or the C_f variation function.

Again it should be reiterated that the defining-equations for ζ, ξ and χ are not dependent on special assumptions as to the particular velocity profile or C_f variations. They remain critical parameters in the film equation for determining the influence of turbulence quantities. They may be used to compare various turbulence "theories" as to differences in their predictions. They are also the quantities to be evaluated by our experimental measurements.